Available online at www.sciencedirect.com
SCIENCE DIRECT
Coastal Engineering 53 (2006) 395–417
Coastal Engineering
An International Journal for Coastal, Harbour and Offshore Engineers
www.elsevier.com/locate/coastaleng

RANS modelling applied to random wave interaction with submerged permeable structures

J.L. Lara *, N. Garcia, I.J. Losada

Ocean and Coastal Research Group, University of Cantabria, Departamento de Ciencias y Tecnicas del Agua y del Medio Ambiente, E.T.S.I. de Caminos, Canales y Puertos, Avda. de los Castros s/n, Santander 39005, Spain

Received 29 March 2005; received in revised form 24 October 2005; accepted 24 November 2005
Available online 18 January 2006

Abstract

This paper is the second part of the work presented by Garcia et al. [Garcia, N., Lara, J.L., Losada, I.J., 2004. 2-D numerical analysis of near-field flow at low-crested breakwaters. Coastal Engineering 51 (10), 991–1020]. In the mentioned paper, flow conditions at low-crested rubble-mound breakwaters under regular wave attack were examined, using a combination of measured data of free surface, bottom pressure and fluid velocities from small-scale experiments and numerical results provided by a VOF-type model (COBRAS) based on the Reynolds-Averaged Navier–Stokes (RANS) equations. This paper demonstrates the capability of the COBRAS model to reproduce irregular wave interaction with submerged permeable breakwaters. Data provided by the numerical model are compared to experimental data of laboratory tests, and the main processes of wave–structure interaction are examined using both experimental and numerical results. The numerical model validation is carried out in two steps. First, the procedure of irregular wave generation is verified to work properly, comparing experimental and numerical data of different cases of irregular wave trains propagating over a flat bottom. Next, the validation of the numerical model for wave interaction with submerged rubble-mound breakwaters is performed through the simulation of small-scale laboratory tests on different incident wave spectra. Results show that the numerical model adequately reproduces the main aspects of the interaction of random waves with submerged porous breakwaters, especially the spectral energy decay at the structure and the spectrum broadening past the structure. The simulations give good results in terms of height envelopes, mean level, spectral shape, root-mean-square height for both free surface displacement and dynamic pressure inside the breakwater. Moreover, large-scale simulations have been conducted, on both regular and irregular incident wave conditions. The overall pattern of the wave interaction with a large-scale submerged breakwater is adequately reproduced by the numerical model. The processes of wave reflection, shoaling and breaking are correctly captured. The good results achieved at a near prototype scale are promising regarding the use of the numerical model for design purposes.

Keywords: Low-crested structures; RANS modelling; Flow in porous media; Irregular wave generation; Irregular wave transformation

1. Introduction

In a previous paper (Garcia et al., 2004a), the flow conditions at low-crested rubble-mound breakwaters under regular wave attack have been examined, using a combination of measured data of free surface, bottom pressure and fluid velocities from small-scale experiments and numerical results provided by a VOF-type model based on Reynolds-Averaged Navier–Stokes (RANS) equations. In the mentioned paper, the employed numerical model, named COBRAS (COrnell BReaking waves And Structures, see Lin and Liu, 1998, Hsu et al., 2002), is proven to correctly reproduce the interaction of monochromatic waves with low-crested permeable structures for different incident wave characteristics and structure freeboards. As an additional step in the validation analysis initiated by Garcia et al. (2004a), Losada et al. (2003) use the same numerical model to investigate the influence of the crest width on the near-field flow pattern and show that the model performs well for another geometric configuration of breakwater. With the aim of demonstrating the model's validity beyond small-scale set-ups, Garcia et al. (2004b) present the simulation using COBRAS of a laboratory experiment on a submerged rubble-mound multilayered breakwater at near-prototype scale. A

* Corresponding author. Tel.: +34 942 201810; fax: +34 942 201860.
E-mail address: lopezjav@unican.es (J.L. Lara).

0378-3839/$ - see front matter © 2005 Elsevier B.V. All rights reserved.
doi:10.1016/j.coastaleng.2005.11.003

satisfying level of agreement is achieved between numerical results and measured data of free surface displacement and bottom pressure at different locations of the wave flume. Computed results of near-structure velocity field are presented and the potentiality of the model for design purposes is emphasised.

Still, the development of a reliable and valid tool for wave–structure interaction requires involving wave randomness. An accurate representation of the structure response under irregular wave attack is of prime importance for engineering design purposes. Very few investigation works on numerical modelling of wave interaction with permeable structures address the randomness of the incident waves. Most of the existing studies propose analytical models for prediction of the structure-induced transformation of non-breaking multicomponent waves. Analytical models have been presented by Massel and Mei (1977) for perforated and porous rectangular emerged breakwaters, by Massel and Butowski (1980) in an extension of the previous work and by Rojanakamthorn et al. (1989, 1990) for submerged permeable structures using an individual wave analysis technique to calculate the transformation of each component of the spectrum. Losada et al. (1996a,b) present two analytical models to analyse irregular wave transformation over and inside a submerged permeable breakwater of arbitrary shape, but do not consider wave breaking. Yoshida et al. (1996) present a numerical method to solve the second-order interaction between a random wave train of arbitrary spectrum and a submerged obstacle and investigate the effect on the transmitted wave spectrum of wave breaking over the obstacle, but do not include structure permeability. The aforementioned analytical models give valuable insight on the behaviour of a breakwater subject to random wave attack, but cannot be viewed as engineering tools for structure design.

Kobayashi and co-workers have presented in a series of publications results of numerical modelling of random wave interaction with impermeable and permeable slopes. Kobayashi and Wurjanto (1989) present a one-dimensional, time-dependent numerical model based on shallow water equations for predicting the flow induced by specified normally incident irregular waves on a rough permeable slope and within a thin permeable underlayer. Kobayashi et al. (1992) show that the numerical model can reproduce, for a known incident wave train introduced as an input, the time series and spectral characteristics of the free surface motion. Kobayashi and Wurjanto (1990) extend the validity of the previous model to underlayers of arbitrary thickness and use the computed results to investigate the interaction processes of irregular waves with thick permeable underlayers. In order to assess the predictive capabilities of the previous authors' improved model, Cox et al. (1994) use the results of the swash zone dynamics measurements of one test on irregular waves from the SUPERTANK Laboratory Data Collection.

Beji and Battjes (1994) use a Boussinesq model with improved dispersion characteristics to simulate regular and irregular wave propagation over a submerged trapezoidal impermeable obstacle. Numerical results for non-breaking waves are compared with laboratory data of free surface displacement time series and spectral density functions, showing good agreement between both types of data. Using a numerical model based on Boussinesq-type equations derived by Schaffer and Madsen (1995), Karambas et al. (1997) simulate irregular wave propagation, including breaking, over a submerged impermeable breakwater, with emphasis put on the energy dissipation due to wave breaking and the energy transfers among wave components. Comparison with experimental data by Beji and Battjes (1994) shows satisfying agreement.

Wei et al. (1999) present results of regular and random wave generation in a Boussinesq-type wave model using a source function method. In order to test the model's validity, comparisons are made with analytical solutions for 2D monochromatic wave propagation in constant water depth, with experimental data for 1D random wave propagation over a constant slope and for 2D monochromatic wave propagation over a constant shoal. For 2D random waves, the authors check that the target wave spectrum over constant depth is correctly reproduced but no results of the model's validation are included.

Avgeris et al. (2004) include the effect of the structure permeability in Boussinesq-type model simulations of irregular wave train propagation over submerged breakwaters. A depth-averaged Darcy equation extended with Forchheimer terms is used to calculate the flow inside the porous structure. Wave generation is achieved using the source function technique described by Wei et al. (1999).

The models based on the complete Navier–Stokes equations using the VOF method to track the free surface have received considerable attention in the last decade for the analysis of wave interaction with coastal structures under breaking conditions, as these models allow the calculation of the velocity field in the whole computational domain for any type of flows, whether rotational or irrotational.

Several works by Van Gent (1994), Iwata et al. (1996), Troch and de Rouck (1998), Kawasaki (1999), Hsu et al. (2002) and Garcia et al. (2004a,b) among others focus on the modelling of wave interaction with permeable structures using models based on the Navier–Stokes equations, and show that these models provide useful information for a deeper understanding, both qualitative and quantitative, of the hydrodynamic conditions in the vicinity of the studied structure. However, all of the aforementioned studies have been carried out taking into account incident regular wave conditions. In a recent study also based on a Navier–Stokes modelling approach, Li et al. (2004) present the simulation of irregular wave interaction with a vertical fixed impermeable barrier in front of a breakwater. Computed free surface displacement time series and velocity field around the vertical barrier are shown as preliminary results. The numerical calculations are not compared with experimental data.

In summary, the previous review shows that most of the existing studies on numerical modelling of random wave interaction with low-crested breakwaters have been conducting using Boussinesq-type models and very few of them take into account permeable structures. Numerical analysis of random wave interaction with submerged structures using a Navier–

Stokes equation (NSE) model seems to be lacking. The aim of the present paper is to demonstrate the capability of a NSE model to reproduce irregular wave interaction with submerged permeable breakwaters. Similarly to the previous analysis on regular waves (Garcia et al., 2004a), the data provided by the numerical model are compared to experimental data of laboratory tests, and the main processes of wave–structure interaction are examined using both experimental and numerical results.

The paper is organised as follows: First, the procedure of irregular wave generation implemented in the model is described and verified to work properly comparing it with experimental data of different cases of irregular wave trains propagating over a flat bottom. Next, the validation of the numerical model for wave interaction with submerged rubble-mound breakwaters is performed through the simulation of small-scale laboratory tests on different incident wave spectra. The numerical results of free surface displacement along the flume and bottom pressure inside the porous breakwater are presented and compared with the corresponding measurements. Finally, the capability of the model to simulate the wave interaction with a porous submerged structure at a scale nearer to the prototype scale is examined. As a preliminary step in the process of the model's validation on random wave conditions at large scale, the analysis focuses first on regular wave conditions, with the simulation of three tests with different water depths, and next, preliminary results of random wave simulation at large scale are presented.

2. Description and validation of the irregular wave generation procedure

2.1. Description of the wave generation procedure

Prior to the simulation of the laboratory tests on random wave interaction with submerged permeable breakwaters, a first effort had to be done to modify and improve the procedure of random wave generation implemented in the initial code of the model. As specified by Lin and Liu (1999), the initial version of the COBRAS model includes the possibility of generating irregular waves as the superposition of n different linear waves, using the following mass source function in the internal wavemaker mode of generation:

$$s(t) = \sum_{i=1}^{n} \frac{C_i H_i}{A} \sin(\sigma_i t - p_{si}) \quad (1)$$

where A is the area of the source region, and C_i, H_i, σ_i and p_{si} are respectively the celerity, height, angular frequency and phase of the ith wave mode. A detailed description of wave generation using an internal wavemaker procedure can be found in Lin and Liu (1999).

The procedure for generation of a random wave spectrum in the modified COBRAS code is described in detail in Appendix A. Modifications of the initial code have been completed to include wave spectrum generation, with the aim of testing the model's ability to reproduce the spectral transformations observed in the laboratory.

2.2. Validation of the wave generation procedure

A series of laboratory experiments have been carried out with the aim of checking the capability of the model to correctly reproduce the generation and propagation of irregular wave trains over a flat bottom. The experiments have been performed in the wave flume of the University of Cantabria (Spain) which is 24 m long, 0.6 m wide and 0.8 m deep. The incident waves are generated with a piston-type wavemaker including an active reflective wave absorption system. Eight wave gauges of resistance-type are placed 5, 5.5, 6.5, 8, 8.15, 8.40, 10 and 11.5 m from the wavemaker (see sketch in Fig. 1). The rear end of the flume is occupied by a wave absorption ramp. Observed

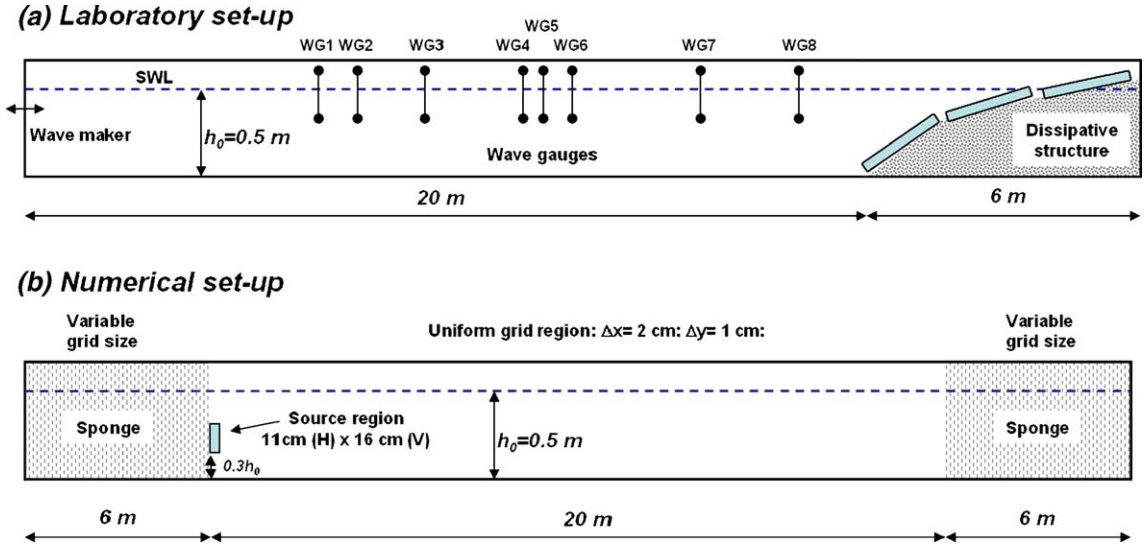

Fig. 1. Sketch of the experimental and numerical setups for the irregular wave simulations.

reflection coefficients from the dissipative ramp in the experiments are lower than 10%. JONSWAP and TMA spectra are generated, with a γ parameter equal to 3.3. The tested significant wave heights H_s range from 7 to 15 cm and the peak periods T_p from 1.6 to 3.5 s, with a 0.50 m still water depth. The cutoff frequencies defined for the generated time series are 0.16 Hz and 1 Hz, according to the restrictions of the wavemaker.

The computational domain designed to reproduce the laboratory experiments faithfully reproduces the experimental set-up, in terms of dimensions of the flume and location and shape of the final obstacle. The grid system is non-uniform in the x-direction, with a minimum cell width of $\Delta x = 2$ cm in the central submesh region, and uniform in the y-direction, with a constant cell height of $\Delta y = 1$ cm in the whole domain. The domain is 32 m long and 0.70 m high, and the total number of cells is 892×70. The source region has been designed applying the rules of thumb included in Lin and Liu (1999) to the spectrum peak period. The sponge layer on the left side, whose length is constant for all the simulation cases, has been checked to properly dissipate the outward-going waves. The sponge layer at the right side of the domain has been designed to simulate the wave damping over the dissipative ramp. Reflection coefficient was evaluated from the numerical simulations to be less than 10%. Similarly to the final slope of the laboratory flume, the final sponge layer of the numerical flume works efficiently as a wave dissipater. The source region is located at the same distance from the first wave gauge as the wavemaker in the laboratory flume. The dimensions of the source region designed for the present study are 11 cm (H) × 16 cm (V). The distance between the bottom of the source region and the flume bottom is taken approximately equal to $h/3$. The irregular time series considered in the numerical calculations are identical to those generated in the laboratory in order to carry out a direct numerical comparison between the computed and measured time series. Free surface at the paddle was calculated from paddle displacements. Wave celerity and wave phases of the measured and simulated irregular wave trains can be compared.

Figs. 2 and 3 show the time series of free surface displacement from the model simulations and from the

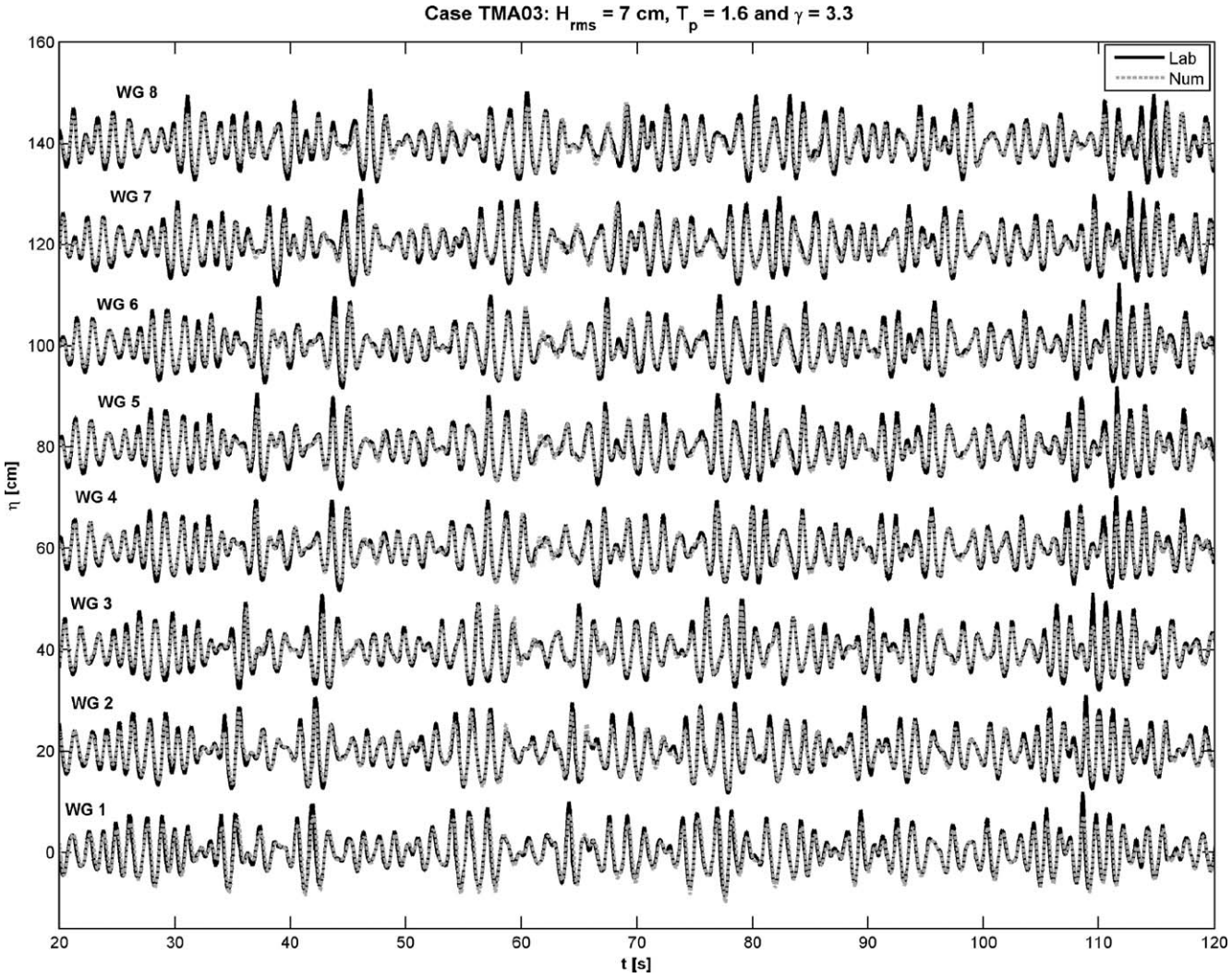

Fig. 2. Free surface evolution (solid line: laboratory measurements, dotted line: numerical computations) for case TMA09: $H_s = 10$ cm, $T_p = 1.6$ s and $\gamma = 3.3$.

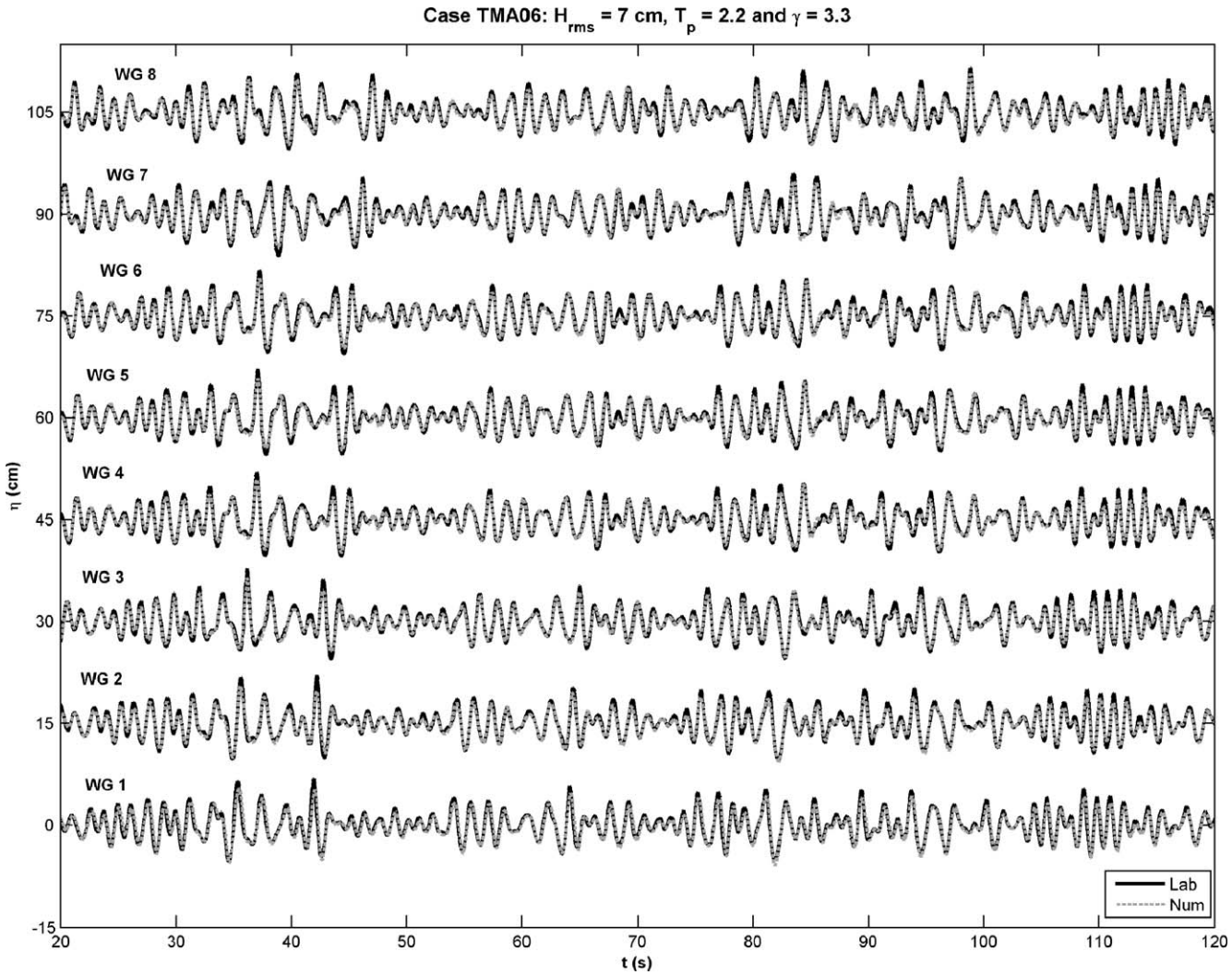

Fig. 3. Free surface evolution (solid line: laboratory measurements, dotted line: numerical computations) for case TMA06: H_s=10 cm, T_p=2.2 s and γ=3.3.

laboratory measurements corresponding to two TMA spectra with similar significant wave heights (H_s=7 cm) but different peak periods, respectively, 1.6 s and 2.2 s. Dotted and solid lines represent numerical results and experimental data, respectively. Although 350 s were simulated for each test, only 100 s are presented in Figs. 2 and 3 for clarity. The overall agreement between numerical results and experimental data for the free surface evolution at the eight wave gauges is seen to be very good. The wave celerity and the wave phases for the simulated wave train are very well reproduced by the model. The measured series of free surface motion are accurately reproduced in terms of wave height, shape and phase at each one of the considered flume sections. However, it can be observed that the model underestimates the height of the highest waves or the height of consecutive short-period waves. The reason of the differences is discussed later on. This fact can be clearly seen in Fig. 2, corresponding to a shorter peak period case, or in Fig. 3 for a group of consecutive small amplitude waves around 95 s.

3. Irregular wave interaction with submerged permeable structures at small scale

3.1. Simulated tests

Validation of the numerical model has been conducted considering the experimental data base on low-crested structures (LCS) described in Garcia et al. (2004a), which includes both regular and irregular wave tests with different values of water depth and characteristics of incident waves. The water depth considered in the two irregular wave tests chosen to be reproduced numerically is the maximum of the three tested values: h=40 cm at the wave paddle. The structure freeboard and crest width are F=−5 cm and b=100 cm, respectively. Two values of peak period are considered: T_p=2.4 s (test 276) and T_p=3.2 s (test 290), while the significant wave height (H_s=10 cm), wave spectrum type (TMA) and peak enhancement factor (γ=3.3) are the same for both tests. Both tests include a flow recirculation system aimed at preventing water piling-up in the leeward side of the low-crested breakwater (see Garcia et al.,

2004a). The total duration of each simulation is set to 200 s in order to achieve time series long enough to fully define the wave spectra.

3.2. Computational mesh

A detailed description of the computational domain can be found in Garcia et al. (2004a). The mesh employed for the irregular wave test simulations presented herein is the same as for simulation of the tests on regular 1.6 s waves described in the aforementioned paper. The grid system is non-uniform in the x-direction, with the minimum cell spacing, $\Delta x=\Delta y=1$ cm being distributed in the vicinity of the breakwater. In the generation zone, the cell dimensions are $\Delta x=4$ cm and $\Delta y=1$ cm. The domain is 26.64 m long and 0.80 m wide and the total number of cells is 1282×82. The area of the source region has been designed applying the rules of thumb described in Lin and Liu (1999) to the spectrum peak period. The sponge layer, whose length is kept unchanged for both simulated tests, has been checked to properly dissipate the outward-going waves. The simulation of the laboratory tests on LCS requires previous calibration of the linear (α) and nonlinear (β) friction coefficients governing the flow inside the porous media and related to the linear and nonlinear drag forces respectively (see Hsu et al., 2002, for equations and nomenclature). As a starting point for the present simulations on irregular wave conditions, the values of the porous flow parameters have been kept constant with respect to those implemented for simulation of the regular wave tests on submerged multilayered breakwaters presented in Garcia et al. (2004a): $\alpha=1000$ and $\beta=0.8$ for the breakwater core, and $\alpha=1000$ and $\beta=1.2$ for the armour layer. As for the regular wave test simulations, these coefficients are not used as tuning parameters but are kept constant for both simulated tests.

3.3. Results of model's validation

In this section, the numerical results of free surface displacement along the flume and bottom pressure inside the porous breakwater obtained in the simulation of the random wave tests are presented and compared with experimental data of upper and lower envelopes and spectral magnitudes.

3.3.1. Free surface displacement

In order to illustrate irregular wave generation and propagation over the submerged porous breakwater, computed results of free surface displacement for test 276 ($T_p=2.4$ s) are presented in Fig. 4. Five sections in the vicinity of the breakwater are considered. A total of 150 s of simulation, from $t=50$ s to $t=200$ s, is presented. Similar to regular wave simulations, random wave conditions can be simulated with no limitations on the computation's total duration. The numerical model simulates wave enhancement due to reflection and shoaling effect (WG5) and breaking (WG6). Most of the computed individual waves display a breaking-wave profile in section 6. High frequency components can be observed in the attenuated wave field of the transmission zone (section 8).

In the case of the present irregular wave simulations, no direct comparison between computed and measured time series can be performed, partly due to the differences in the mode of wave generation used in the laboratory and in the numerical flume. The irregular waves are generated using an

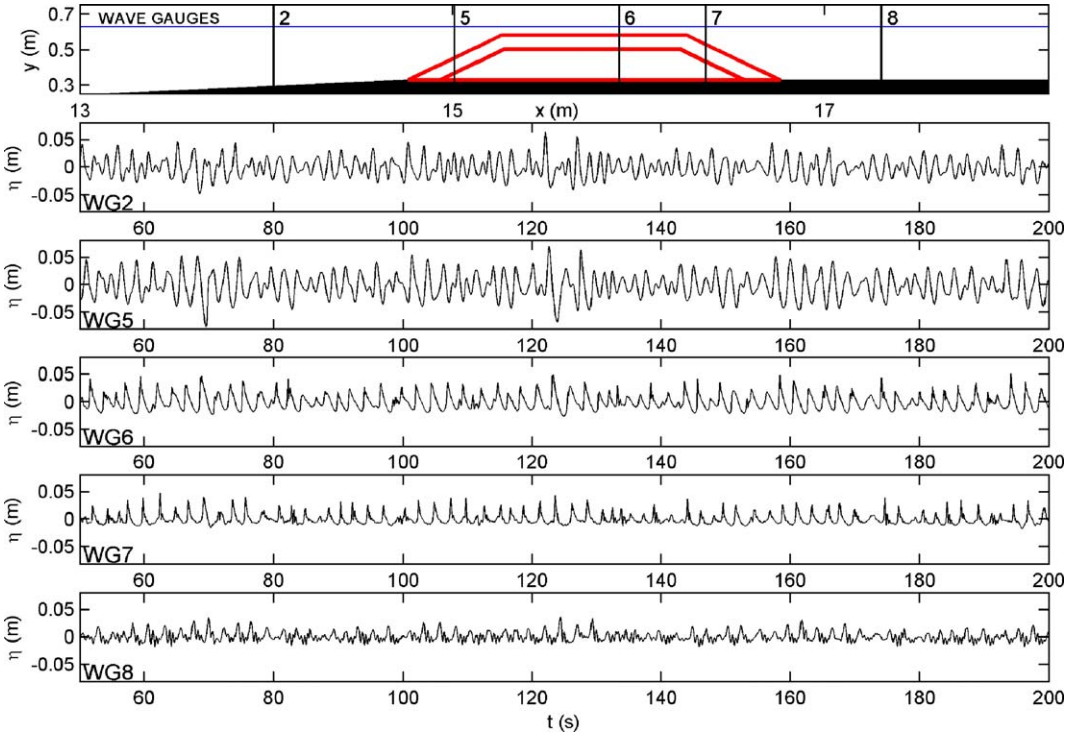

Fig. 4. Computed time series of free surface displacement in the vicinity of the submerged breakwater. $F=-5$ cm, $b=100$ cm, $H_s=10$ cm, $T_p=2.4$ s.

internal wavemaker, with the source region placed one wavelength (for significant wave period) seaward of the location of the wave paddle in the laboratory, in order to fulfil the flow regularisation requirement. This results in different wave phase evolutions between the experimental and numerical flumes. Furthermore, the present simulations do not consider measured wave series as inputs, but are performed using the wave generation procedure based on the target wave spectrum characteristics. Consequently, due to the random nature of the simulated waves, the numerical results of surface displacement cannot be verified through a direct comparison with the measured series.

However, it has to be mentioned that the numerical model can be used to reproduce measured time series under irregular wave conditions. This requires to introduce as input data for wave generation the wave components obtained from a Fourier analysis of the time series measured at a given gauge and to define the source region at the same location as the considered gauge. Such results will not be shown here, as the objective of the present section is to test the capacity of the model to simulate adequately the generation and propagation of incident irregular waves using as input data the parameters of a given TMA spectrum: water depth in generation, root-mean-square or significant wave height, peak period and peak enhancement factor. Hereafter, the validity of the numerical results is tested based on data of wave height envelopes, mean water level and spectral parameters.

Fig. 5 presents the numerical results and experimental data of wave height envelopes and mean water level for the two simulated tests. The pattern of wave height evolution is seen to be well captured for both tests. The root-mean-square error on the wave height at the 11 sections of measurement is lower than 9% and 8% for test 274 (T_p=2.4 s) and 290 (T_p=3.2 s), respectively. The modulation of the wave height envelopes in the seaward region due to partial reflection at the breakwater and the breaking-induced wave decay over the structure crest are well described by the numerical model. The transmitted wave heights are in good agreement with the corresponding measurements. The spatial variations of the mean water level are also correctly computed.

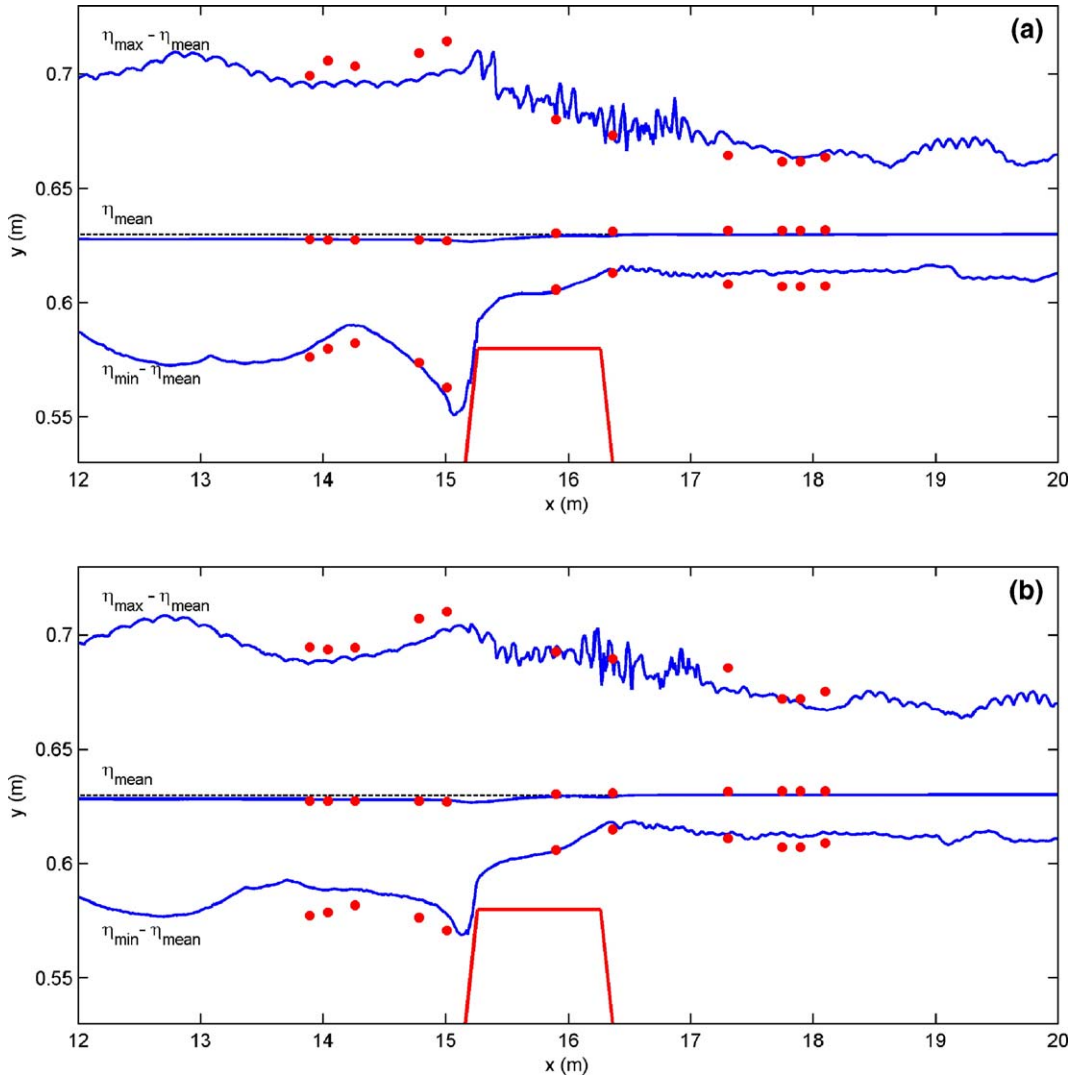

Fig. 5. Computed envelopes and mean water level. Numerical calculations: solid line, experimental data: dots. F=−5 cm, b=100 cm, H_s=10 cm, (a) T_p=2.4 s, (b) T_p=3.2 s.

The wave spectrum evolution along the flume is presented in Figs. 6 and 7. An accurate description of the spectral evolution of the incident waves is essential for a correct assessment of the breakwater performance. As commented in Garcia et al. (2004a), transmission at low-crested structures induces a reduction of the total incident wave energy, but also a redistribution of the remaining energy in the frequency domain. The knowledge of the transmitted spectrum characteristics is of great interest for design purposes, in order to estimate for instance the morphological response of the beach protected by the considered structure. Figs. 6 and 7 correspond to tests 276 and 290, respectively, and illustrate the spectral changes taking place as the incident waves interact with the permeable submerged breakwater. The solid and dotted lines represent the measured and computed spectra respectively. In order to allow a better visualisation of the low energy transmitted spectra, the vertical scale of the graphs corresponding to the seaside sections (WG7 to WG11) is amplified for each of the two figures.

The numerical model is able to correctly reproduce the measured spectrum at each one of the considered sections. A good description of the incident wave train spectral evolution is obtained in terms of energy peaks location and spectral shape. The numerical model adequately reproduces the main characteristics of the wave spectrum transformation over the submerged porous breakwater. Wave spectra at sections 4 and 5 display a significant enhancement of the energy peak, corresponding to the reflection-induced standing wave pattern and shoaling effect over the seaward slope of the breakwater. A considerable reduction of the incident wave energy is achieved past the submerged structure, due to wave breaking over the structure and dissipation inside the porous media. At section 7 and following sections, the energy is carried out at a wider range of frequencies as a result of energy transfer to higher frequencies as the incident irregular wave train propagates over the submerged breakwater. The numerical model is seen to reproduce very well the broadening of the wave spectrum past the submerged structure.

It can be noticed that, at the seaside sections (1 to 5), the high frequency part of the spectrum is slightly underestimated by the numerical model. This feature is believed to be related to the employed mode of wave generation. With the internal wave-maker procedure, based on a source region inside the fluid domain, the highest frequencies are "cutoff" from the generated wave spectrum. As described in Lin and Liu (1999), the waves are generated in response to the introduction of mass in the cells defining the source region: fluid particles are alternately pushed upward out of the source region and sucked into it, generating

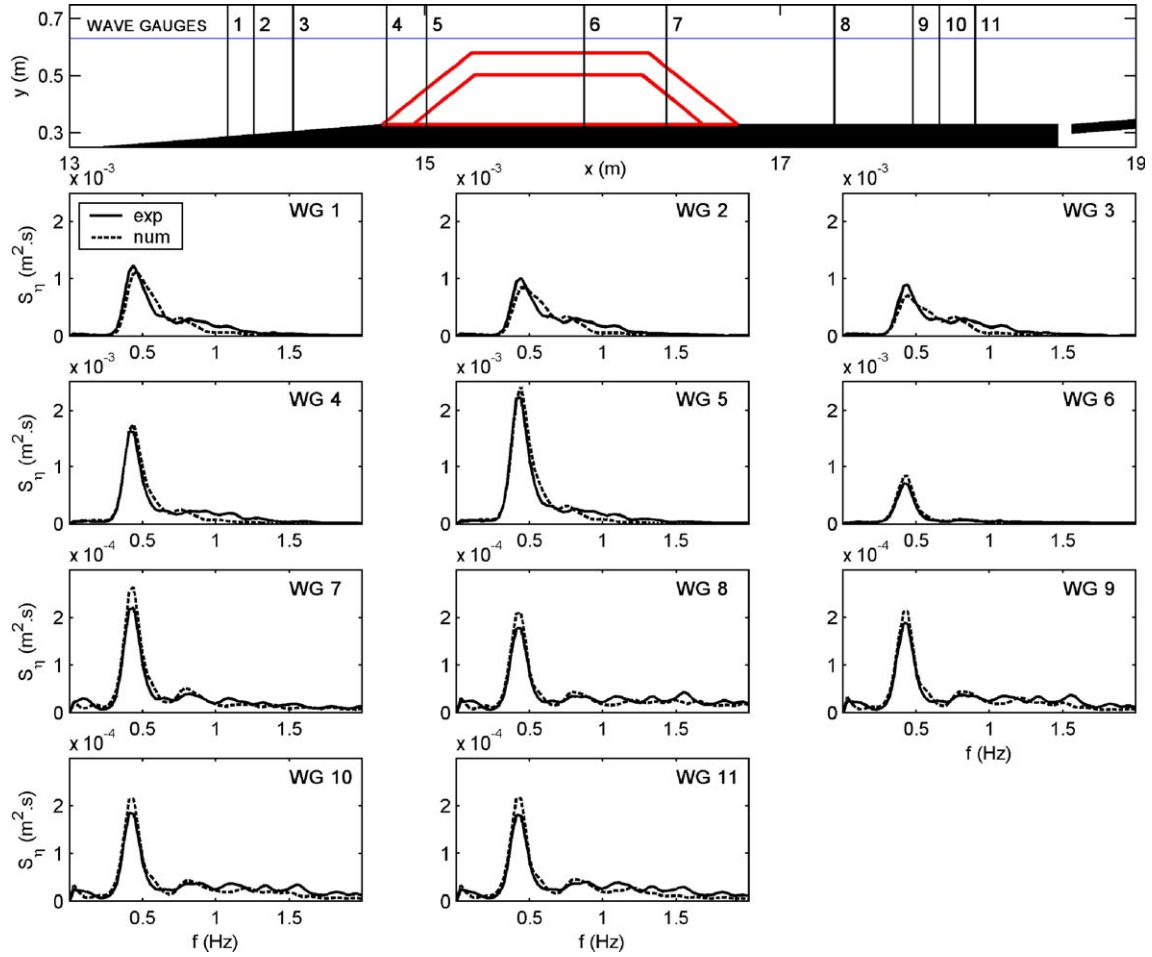

Fig. 6. Spatial evolution of the wave spectrum. $F=-5$ cm, $b=100$ cm, $H_s=10$ cm, $T_p=2.4$ s.

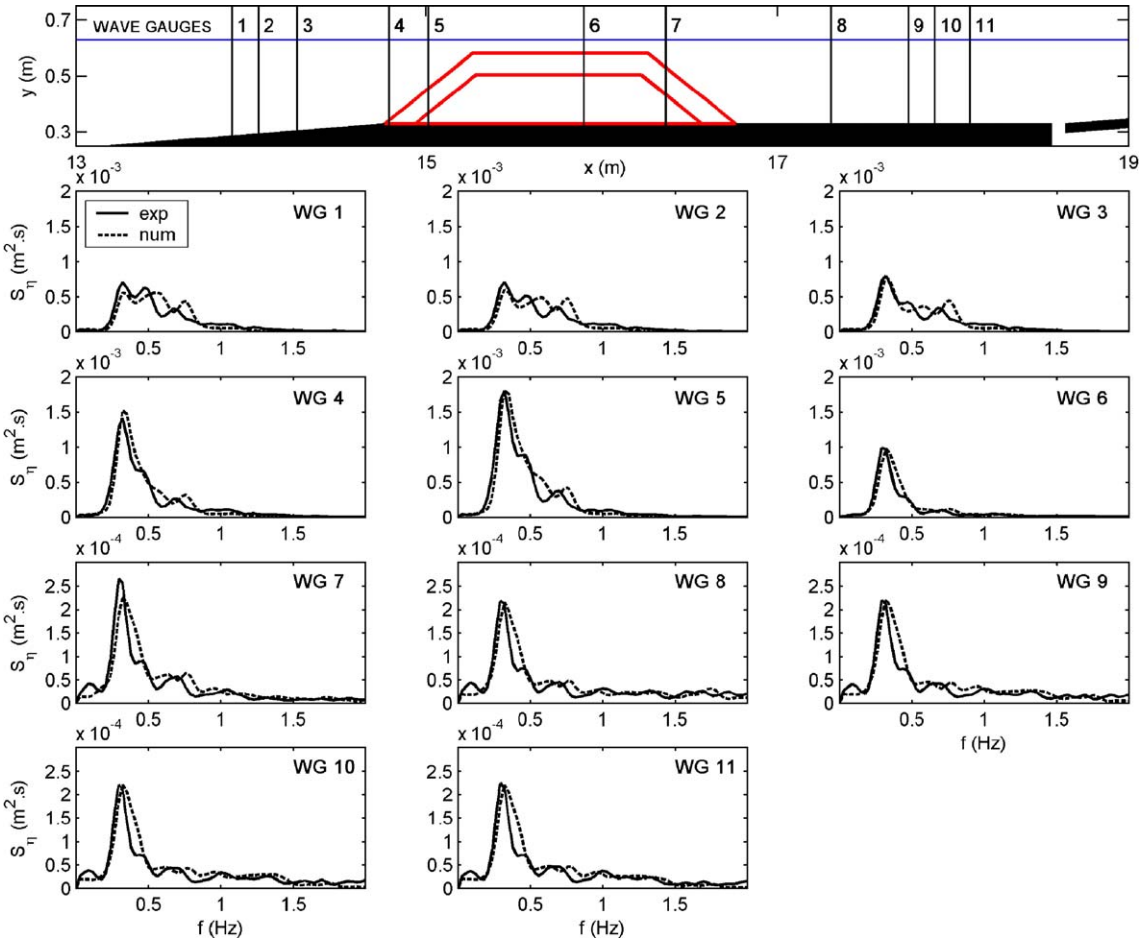

Fig. 7. Spatial evolution of the wave spectrum. $F=-5$ cm, $b=100$ cm, $H_s=10$ cm, $T_p=3.2$ s.

above the source region respectively the crest and the trough of gravity waves. The internal wavemaker formulation is based on waves propagating in shallow waters, where the mass flux is evaluated as: mass flux $=Uh=c\eta$. Following this assumption, the flow is assumed quasi-uniform in the vertical. Hence, the rules of thumb described in several works, which use the internal wavemaker procedure, are suitable to generate waves that propagate in intermediate or shallow waters. Using this procedure, the high frequency wave components of the spectrum, which propagates in deep water, cannot be generated together with the lower frequency part of the spectrum. Numerical tests varying the mesh resolution in the wave generation zone have been performed to assess the influence of the grid size on this feature. No improvements in the results were achieved using finer meshes. Additional tests were performed to test the influence of the location and the dimensions of the source region and have shown in particular that even with the source region located close to the surface, the high frequency components of the incident spectrum could not be generated. Hence, the inaccurate simulation of the highest frequencies of the incident wave spectrum is ascribed to the aforementioned wave generation issue related to the internal wavemaker mode of generation and not to a lack of numerical resolution or an incorrect design of the source region. It is interesting to note that, though the high frequency part of the incident spectrum is poorly described, the numerical model is able to simulate the spectrum widening past the breakwater related to energy transfers to high frequency components.

In the following figures, the spatial evolution of the main parameters of the wave spectrum is presented. Figs. 8 and 9 correspond to tests 276 and 290, respectively. In each figure, the location of the wave gauges is recalled on the first panel. On the following three panels, the spatial evolution of the root-mean-square wave height H_{rms}, of the spectrum peak period T_p and of the Longuet-Higgins (1975) spectral width parameter ν, measured in the laboratory (dots) and calculated by the model (solid lines), is plotted. The root-mean-square wave height H_{rms} and the Longuet-Higgins (1975) spectral width parameter ν are defined by the following expressions:

$$H_{rms}=\frac{4.004\cdot\sqrt{m_0}}{1.416} \tag{2}$$

$$\nu=\left[\frac{m_0m_2}{m_1^2}-1\right]^{1/2} \tag{3}$$

with m_0, m_1 and m_2 being the zeroth, first and second spectral moments of the frequency spectrum, respectively.

The spatial evolution of H_{rms} illustrates the energy damping at the structure. For both tests, an abrupt decrease

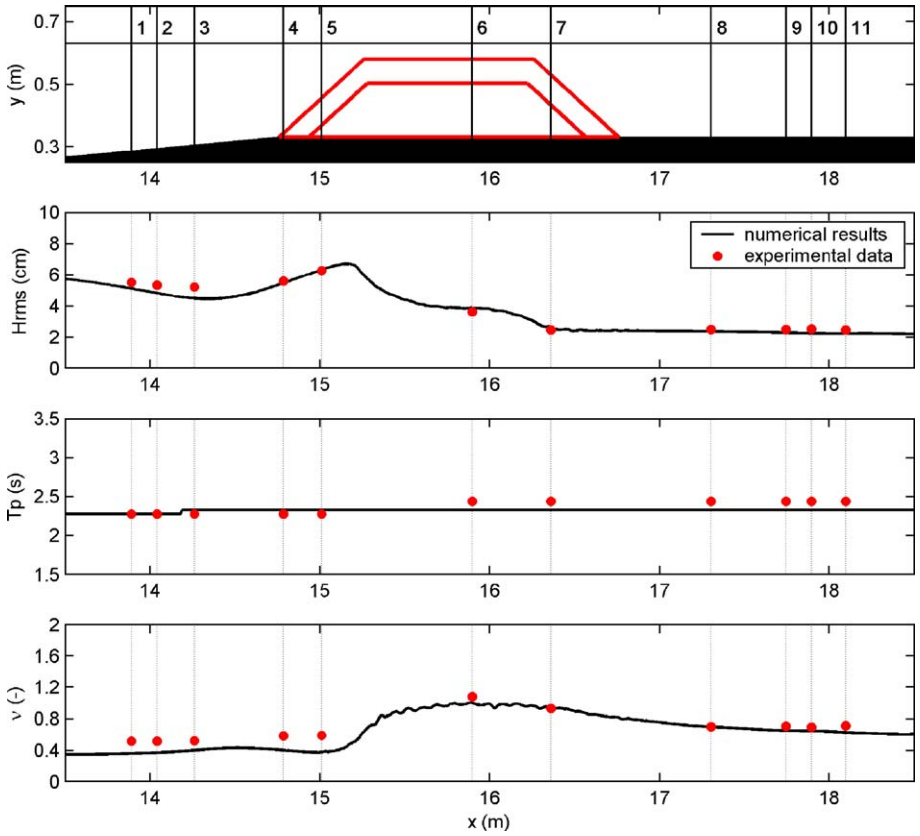

Fig. 8. Spatial evolution of spectral magnitudes. $F=-5$ cm, $b=100$ cm, $H_s=10$ cm, $T_p=2.4$ s.

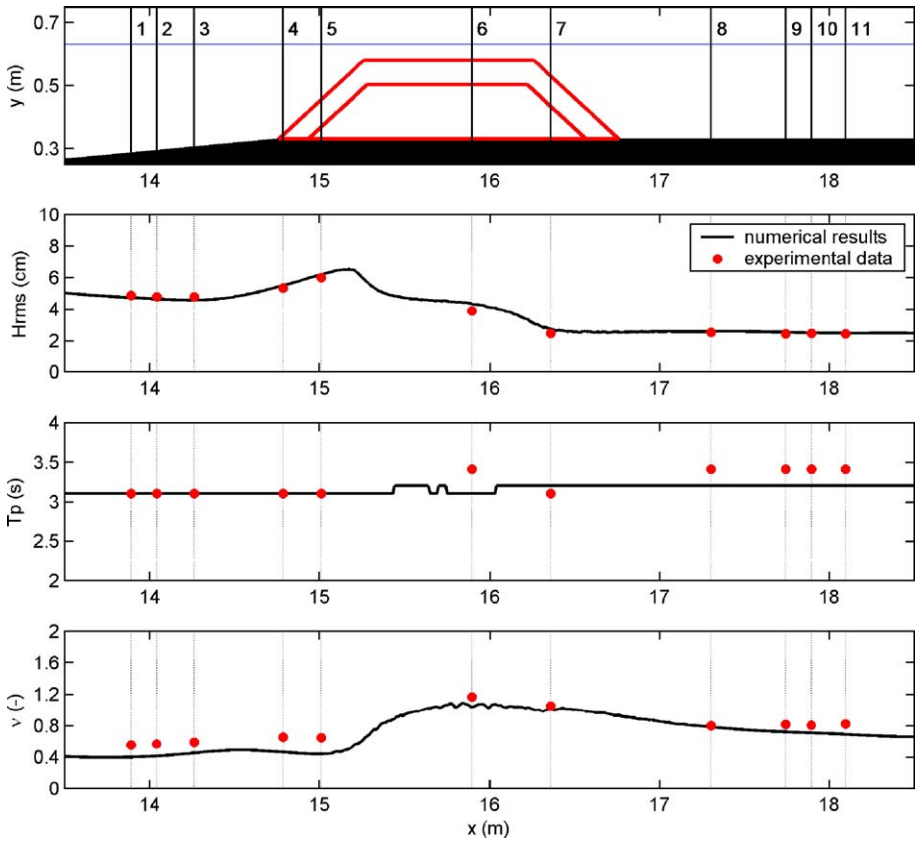

Fig. 9. Spatial evolution of spectral magnitudes. $F=-5$ cm, $b=100$ cm, $H_s=10$ cm, $T_p=3.2$ s.

is observed from the outer edge of the structure crest due to wave breaking. The root-mean-square wave height then remains nearly constant in the leeside zone, with the total energy no longer being dissipated, but redistributed due to nonlinear interactions between the different wave components. The degree of agreement between both experimental and numerical data is very satisfying for both tests, with a root-mean-square error at the 11 considered sections lower than 9%. Regarding the spatial evolution of the peak period T_p, it can be seen that this parameter remains almost unchanged all along the flume. Numerical results of peak period agree very well with the experimental data, with a root-mean-square error in the computation of T_p of 4% and 8% for tests 276 and 290, respectively. Among the various existing parameters to characterise the width of the wave spectrum, see Van Vledder (1992) for a review, the spectral width parameter ν defined by Longuet-Higgins (1975) is one of the most commonly used.

The overall trend of the spectral width spatial evolution is rather well reproduced by the numerical model. As observed in both numerical results and experimental data, the wave spectrum broadens over the submerged structure (see sections 6 and 7) but narrows past the obstacle due to breaking, resulting eventually slightly wider in the transmission zone than in the seaward zone. As can be observed in the two figures, a good level of agreement between computed and measured values is achieved in the region of the breakwater crest and in the leeside zone. Numerical results are less accurate in the seaward zone: the spectral width calculated by the numerical model is rather underestimated, for the aforementioned wave generation procedure-related reasons.

3.3.2. Internal pressure

A similar comparative analysis is performed with data of bottom pressure inside the breakwater. As an example of computed results, Fig. 10 displays the time series of dynamic pressure inside the porous breakwater at the interface with the flume bottom for case 276 (T_p=2.4 s). The location of the gauges, separated 50 cm from one another, is shown in the first panel of the figure. Fig. 11 presents the envelopes of the pressure inside the breakwater as well as the pressure mean value of dynamic pressure for the two simulated tests. Pressure height decreases substantially along the structure, with the recorded heights at gauges 2 and 3 being about 41% and 59% lower, respectively, than at gauge 1 for test 276 (T_p=2.4 s) and 33% and 54%, respectively, for test 290 (T_p=3.2 s). The computed data agree very well with the measurements for each of the two simulated tests. The numerical model accurately reproduces the internal pressure decrease as the distance from the outer face of the structure increases. The root-mean-square error on the maximum pressure in the three sections of measurement is lower than 16% and 5% for test 274 (T_p=2.4 s) and 290 (T_p=3.2 s), respectively.

Fig. 12 presents the pressure spectra at the three points of measurement and illustrates the capacity of the numerical model to simulate the main spectral characteristics of the random wave-induced bottom pressure inside the porous breakwater. The spectral density peak is correctly captured for the two simulated tests, in terms of both location and magnitude. The shape of the pressure spectra is also rather well reproduced and the pressure damping along the breakwater core can be clearly observed on both computed and measured data. Compared with the spectra of free surface displacement, a better description of

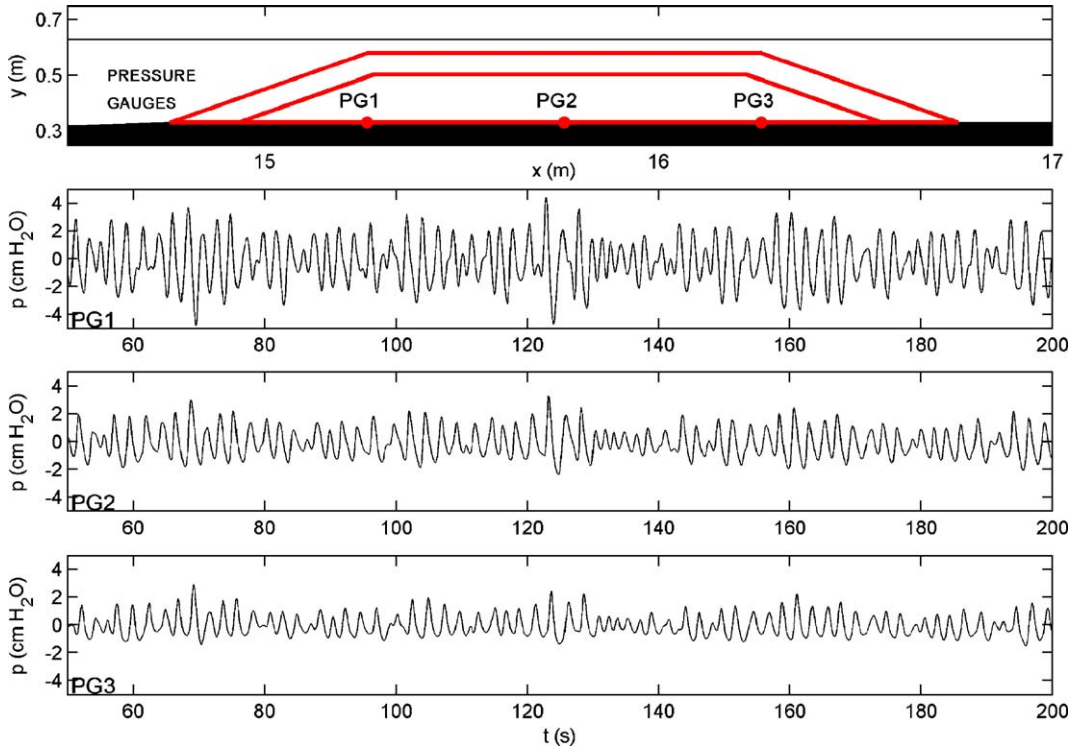

Fig. 10. Computed time series of internal pressure. F=−5 cm, b=100 cm, H_s=10 cm, T_p=2.4 s.

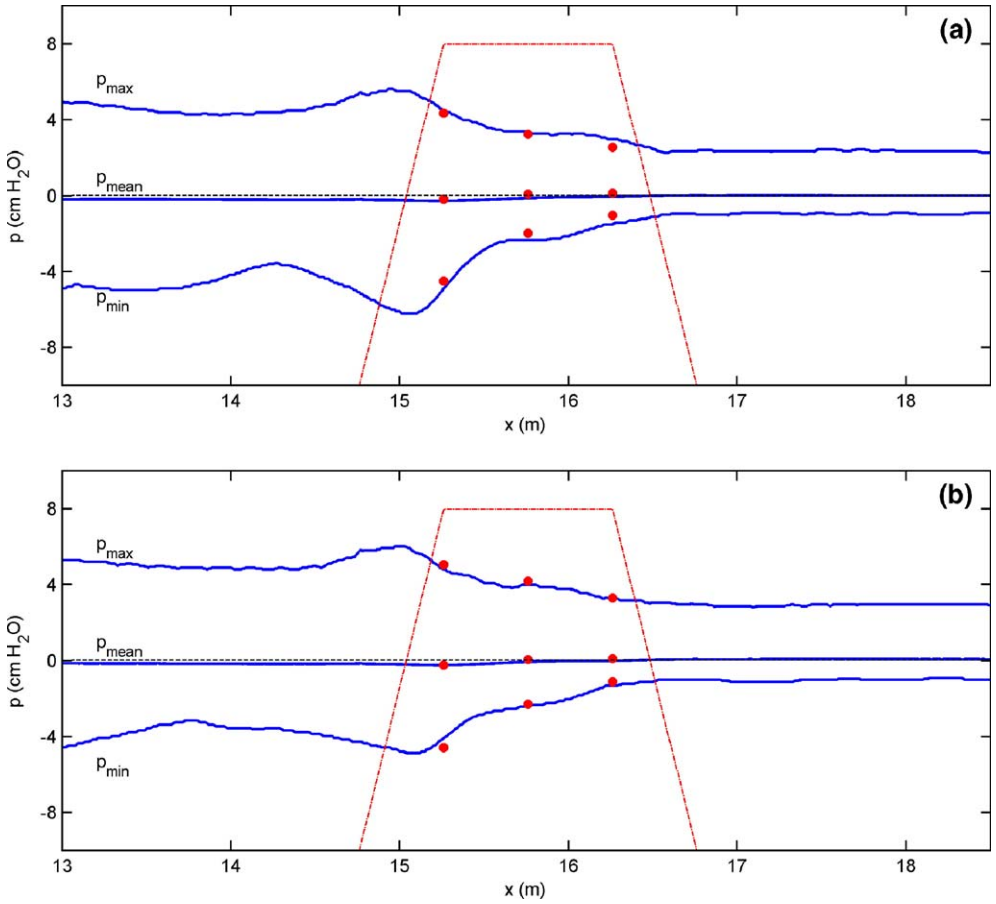

Fig. 11. Dynamic bottom pressure envelopes and mean value. $F=-5$ cm, $b=100$ cm, $H_s=10$ cm, (a) $T_p=2.4$ s, (b) $T_p=3.2$ s. Numerical calculations: solid line, experimental data: dots.

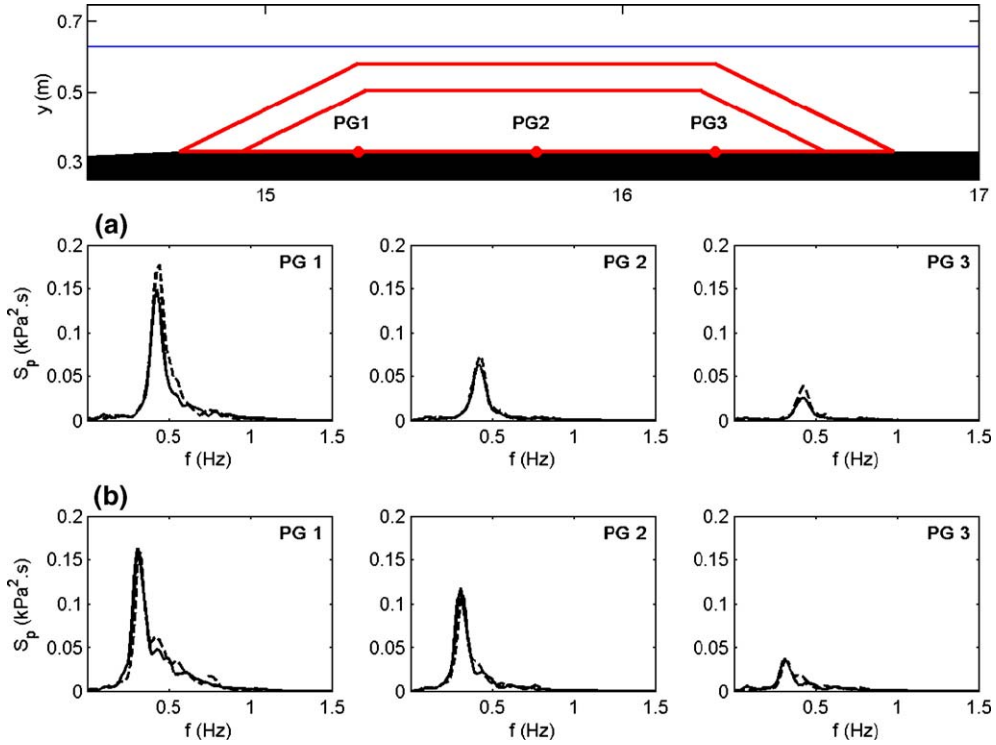

Fig. 12. Dynamic pressure spectra. $F=-5$ cm, $b=100$ cm, $H_s=10$ cm, (a) $T_p=2.4$ s, (b) $T_p=3.2$ s.

the spectrum shape is achieved, as the higher frequency components, poorly described by the numerical model, are damped inside the porous media.

Similarly to the figures shown for the free surface spectra, Fig. 13 presents the results of spatial evolution of the root-mean-square pressure height p_{rms}, the peak period T_p of the pressure spectra and the spectral width parameter ν for the two considered tests. The damping of the internal pressure is seen to be very well captured independently of the tested incident spectrum, with a root-mean-square error on the root-mean-square pressure height at the three points of measurement lower than 10% for both tests. The peak period is seen to be roughly constant at the three considered points inside the breakwater and is also very well captured, with a root-mean-square error lower

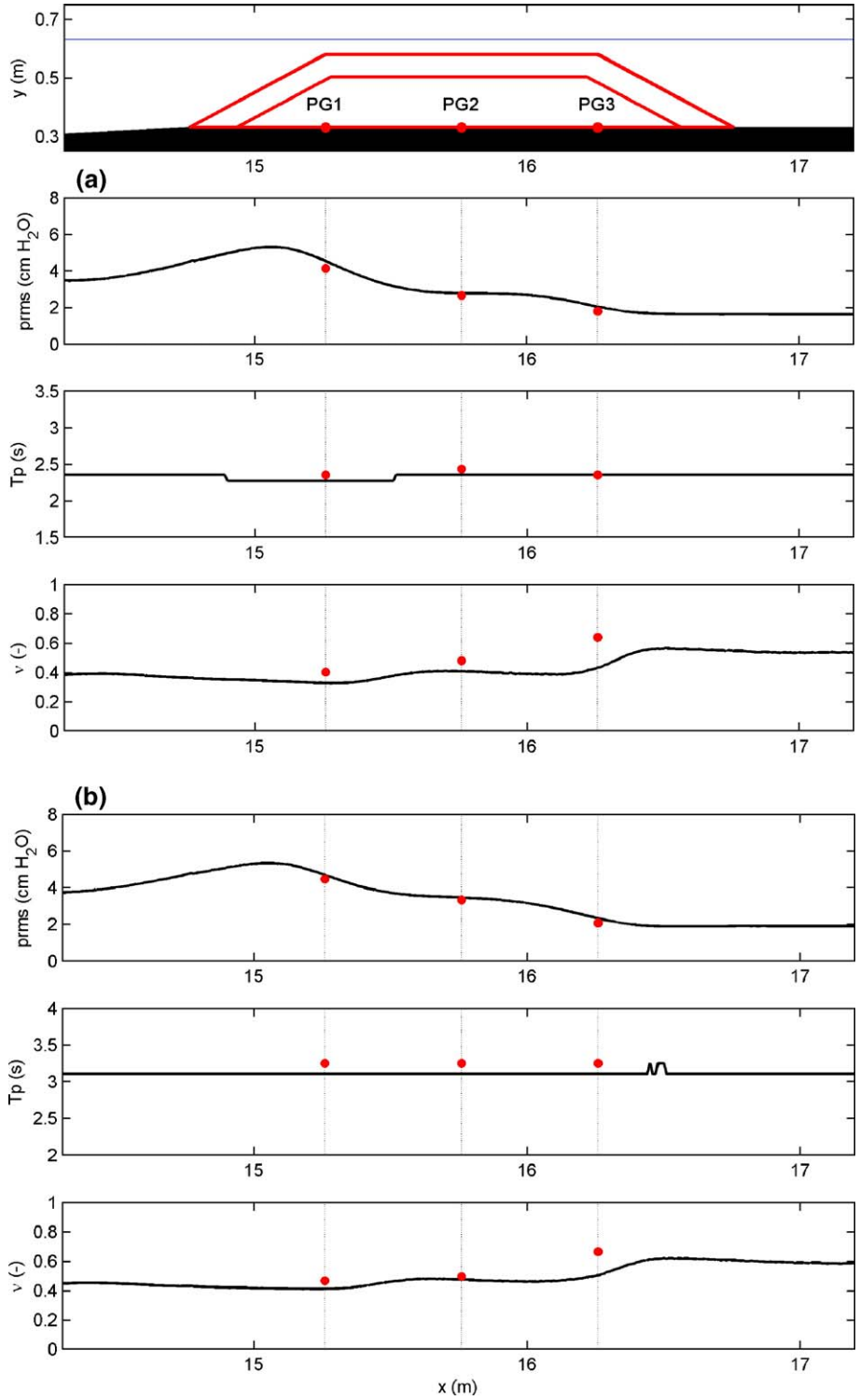

Fig. 13. Spatial evolution of spectral magnitudes. $F=-5$ cm, $b=100$ cm, $H_s=10$ cm, (a) $T_p=2.4$ s, (b) $T_p=3.2$ s.

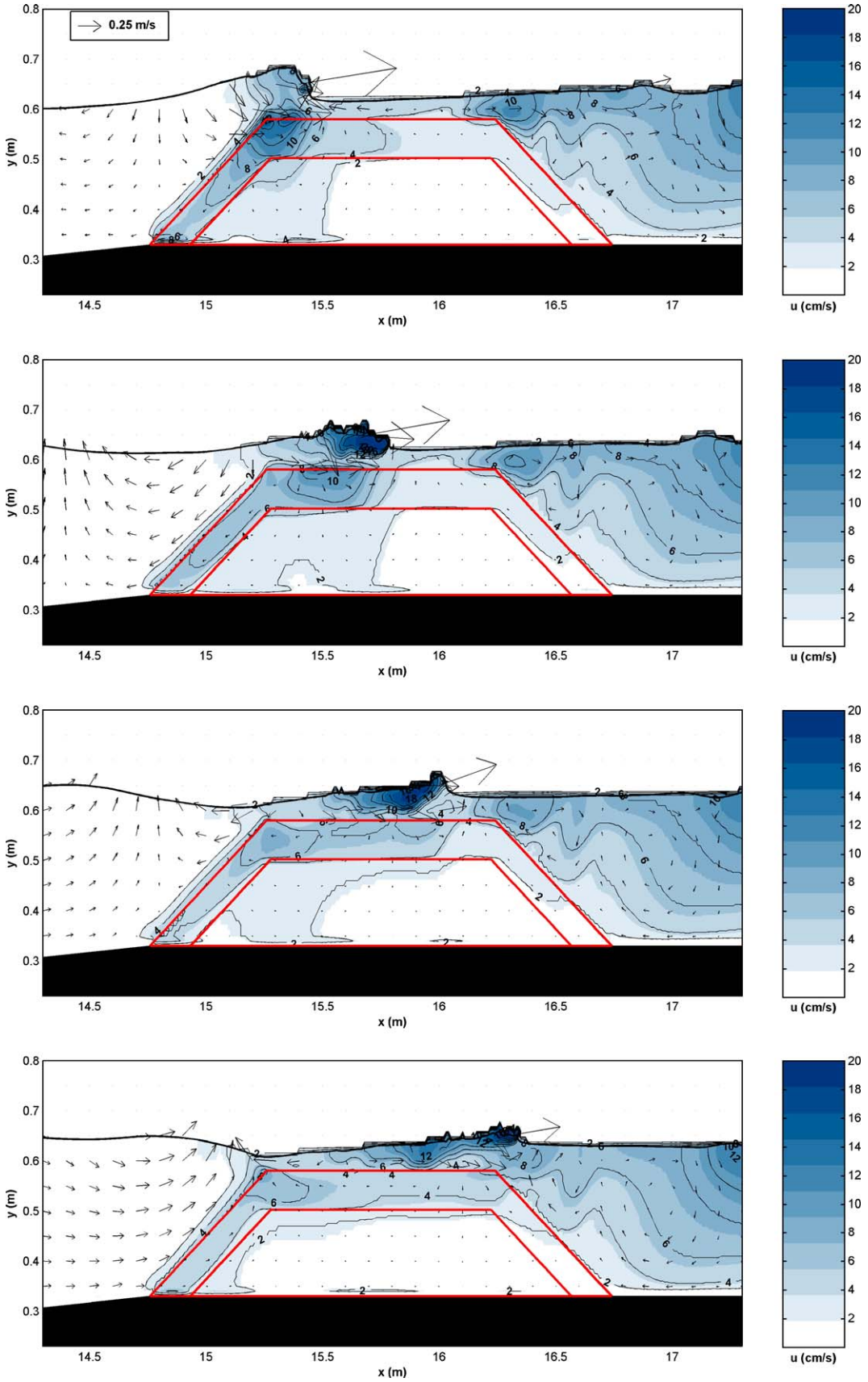

Fig. 14. Computed turbulent intensity and velocity field under breaking wave. $F=-5$ cm, $b=100$ cm, $H_s=10$ cm, $T_p=2.4$ s (test 276). Elapsed time between snapshots: 0.3 s.

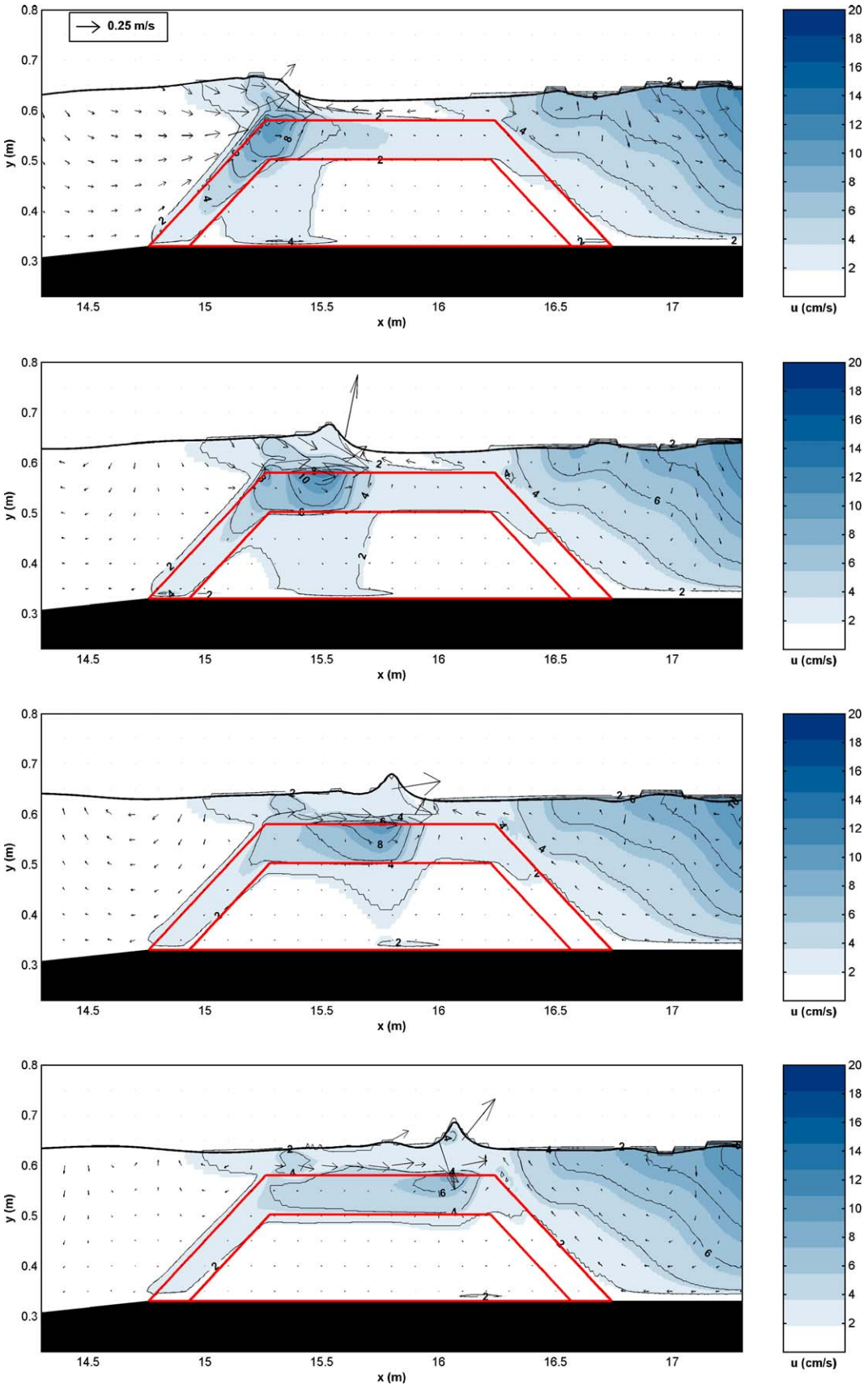

Fig. 15. Computed turbulent intensity and velocity field under non-breaking wave. $F=-5$ cm, $b=100$ cm, $H_s=10$ cm, $T_p=2.4$ s (test 276). Elapsed time between snapshots: 0.3 s.

than 5% for both tests. The spectral width ν is seen to be lower in the case of the pressure spectra, as a result of the high frequency damping inside the porous media.

3.3.3. Turbulence intensity and velocity fields

In this section, as an example of application of the numerical model, computed results of turbulence intensity and velocity fields around and inside the submerged structure are presented.

The knowledge of the distribution and magnitude of water particle velocities around the breakwater is essential for the analysis of the structure's stability. The assessment of the armour stones' stability using quasi-empirical models for instance, based on wave-induced forces parameters derived from Morison-type equations or expressed in terms of bed shear stress (see e.g. Vidal et al., 1998, for near-bed rubble-mound structures), requires information of the flow conditions in the vicinity of the structure. Besides, information concerning turbulence intensity is of great interest for assessment of the ecological impact of the breakwater, as the level of turbulence near the structure is a factor influencing the settlement of epibiotic communities. The knowledge of the distribution of flow velocity and turbulence intensity in the structure vicinity allows the identification of potential habitats for epibiotic species and the assessment of survival potentialities (Denny, 1988). The presented results correspond to the simulation of test 276 (T_p=2.4 s).

Two series of snapshots are presented, illustrating the propagation of a breaking wave, Fig. 14, and a non-breaking wave, Fig. 15, over the submerged breakwater. The results of turbulence are presented in terms of turbulence intensity, defined as $u = \sqrt{2k}$ where k is the computed turbulent kinetic energy (TKE). In Fig. 14, the highly concentrated turbulence energy intensity at the crest of the broken wave can be observed. The model is able to simulate the turbulence processes associated with wave breaking over the breakwater, with turbulence intensity reaching maximum values over the trough region and being spread by the bore in the onshore direction over the crest of the structure. The largest values of fluid particle velocities are achieved above the structure crest, in the region of the breaking wave crest. The particle velocities calculated in the porous media are negligible compared to the values in the fluid region.

Turbulent intensities are also calculated within the breakwater. The highest values of the internal turbulence intensity are computed in the outer layer of the structure. A large vertical velocity gradient is developed at the interface with the fluid region, giving rise to high turbulent levels. Maximum values are observed at the seaward edge of the breakwater crest, before the wave breaks, as flow constriction induces high water particle velocities, enhancing the vertical velocity gradient and thus, the turbulence energy intensity. This feature can be seen in the first panel of Fig. 14, where values of u around 12 cm/s are observed at the seaside vertex of the structure. For the given incident wave conditions and structure characteristics, much smaller values are calculated in the structure core, with values lower than 6 cm/s being predicted for the whole wave period.

The presence of the submerged obstacle does not cause all the waves forming the simulated sea state to break, as can be seen in Fig. 15. The four snapshots illustrate the propagation of the wave immediately following the breaking wave shown before. The impinging wave progressively deforms and steepens while travelling over the structure crest and reaches the deeper waters of the leeside zone without breaking. In this case, the turbulence production inside the porous media is predominant. The maximum value of turbulence intensity is observed as in the previous case when the wave crest reaches the seaward edge of the structure crest.

4. Wave interaction with LCS at large scale

In Garcia et al. (2004a) and in the previous section of the present paper, the capability of the numerical model to reproduce the processes involved in the wave interaction with porous low-crested breakwaters has been proven through a calibration/validation procedure based on small-scale simulations for regular and irregular wave conditions. The scale of the structure modelled in the laboratory experiments and corresponding numerical simulations was approximately 1:20. In the present section, the capability of the model to simulate the wave–structure interaction processes at a scale nearer to the prototype scale is examined. The analysis is based on data of large-scale laboratory experiments performed on a 1:3 LCS model.

4.1. Description of experiments and numerical simulations

Similarly to the small-scale tests considered in the previous section and extensively described in Garcia et al. (2004a), the large-scale laboratory experiments considered herein were performed in the frame of the DELOS ("environmental DEsign of LOw-crested coastal defence Structures") European Project. The experiments were carried out at the Maritime Engineering Laboratory of the Polytechnic University of Catalunya (Spain), in a 100 m long, 3 m wide and 5 m deep wave flume. The general configuration of the experiments is presented in Fig. 16.

During the tests, the bottom of the flume was rigid and presented a multisegmented profile. The LCS model was built on the horizontal section of the bottom, in the central part of the flume. The rear part of the flume was occupied by a dissipative parabolic beach built with homogeneous natural stones, with a 0.5 kg specific weight, aimed at preventing multireflection effects leeward of the structure. The hydraulic wave generation system includes a wedge-type paddle made of aluminium that slides up and down on a 30° inclined plane. Similarly to the structure tested in the DELOS small-scale experiments performed at the University of Cantabria (Spain), the structure employed in the large-scale tests was composed of a core protected by a two-layer armour. The core was made of quarry limestone, with a diameter between 20 and 40 mm and a specific weight of 2.65 T/m^3. This material was covered with two layers of natural stones of the same origin, with the following characteristics of weight and size: W_{50}=3.36 kg, D_{n50}=10.82 cm, W_{85}/W_{15}=2.05 and D_{85}/

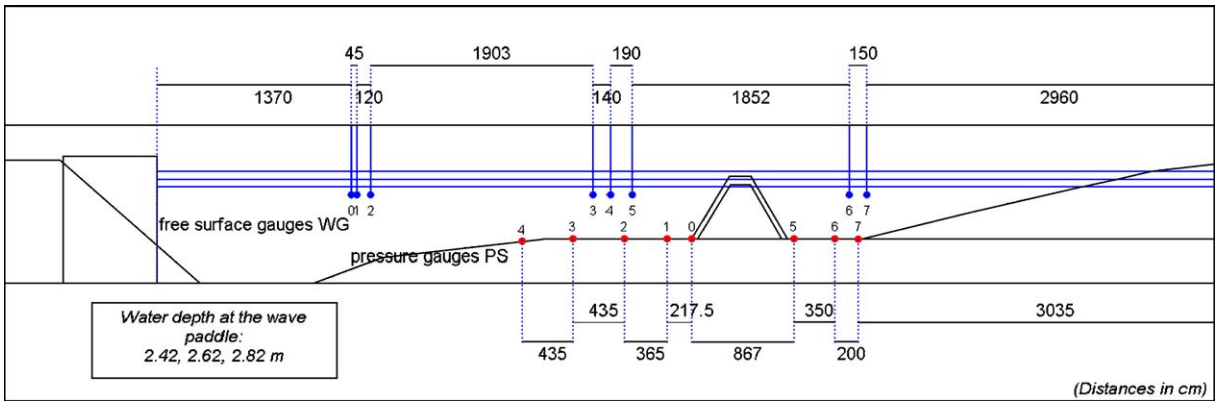

Fig. 16. General sketch of the large-scale experimental set-up.

$D_{15}=1.27$. The main characteristics of the model geometry are summarised in Table 1.

A total of eight resistive wave gauges were placed all along the flume: three near the wave paddle to control the wave absorption system, three in front of the model (seaward zone) and two behind (leeward zone). A total of eight pressure gauges were placed on the bottom of the flume, five in front of the structure and three behind, across a distance greater than the expected wave length.

A total of 63 wave tests were performed on both regular and random waves. The random wave conditions were selected according to the real mean conditions observed on the Catalan coast (West Mediterranean Sea). JONSWAP spectra with peak factor $\gamma=3.3$ were used. The tested significant wave heights and peak periods ranged between 21 and 40 cm, and 2.18 and 3.11 s, respectively. All wave conditions were generated for three water level conditions, corresponding to structure freeboards of −13, 7 and 27 cm.

The computational mesh designed for the simulation of the large-scale laboratory tests is presented in Fig. 17. The experimental set-up, including a multisegmented flume bottom and the LCS located on the horizontal section of the flume bottom, was strictly reproduced. The initial slope is made of three segments of decreasing slope. The modelled breakwater, as in the small-scale experiments, is made of two different porous media. The parabolic dissipative beach built at the rear end of the flume to prevent multireflection effects behind the structure is also included in the numerical set-up. The location of the free surface and pressure gauges as well as the three values of tested water depth are recalled in Fig. 17(b). Contrary to the small-scale test configuration, no flow recirculation system is included (see Garcia et al., 2004a).

Table 1
Details of the tested LCS cross-section

Crest width (m)	1.215, 1.825
Crest height (m)	1.59
Front and back slopes	1V:2H
Freeboard (m)	−0.13, 7, 27
Armour stone size (m)	$D_{n50}=0.108$
Core stone size (mm)	20/40
Armour layer thickness	$2D_{n50}$

The employed values for the porous flow parameters are, in a first attempt, chosen to be identical to those calibrated and validated at small scale. Hence, two values of the β parameter are used for the structure core depending on whether the tested breakwater is submerged ($\beta=1.2$) or emerged ($\beta=0.4$), while the β parameter for the armour layer and the α parameter for both porous media are set constant to $\beta=1.2$ and $\alpha=1000$ independently of the tested water depth. An additional difficulty of the large-scale experiment simulation is the presence of the final rubble-mound slope, and hence a third porous medium to be modelled. As a starting point of the simulations, the porous flow parameter values considered for the dissipative beach are $\alpha=1000$ and $\beta=1.0$, which are values included in the ranges tested in the previous regular and irregular simulations and in previous simulations reported in the literature.

The designed computational mesh is divided into three regions of different resolutions, corresponding to the wave generation zone, the breakwater vicinity and the absorbing beach. The length of the computational domain is 99.2 m × 1.80 m. The entire domain is discretised into a 1635 × 72 grid system with a uniform grid in the y-direction, $\Delta y=5$ cm, and a non-uniform grid in the x-direction. The finest cell spacing is defined in the vicinity of the breakwater, where 5 cm × 5 cm computational cells are used. The cell width in the wave generation region is not constant, varying from 12 cm at the leftward boundary to 5 cm in the zone of interest. Similarly, in the rightward region, with no high resolution requirements, the grid is not uniform, with a maximum cell width of 40 cm at the final boundary of the mesh. A sponge layer of approximately one wave length (8 m) is included for dissipation of the outgoing waves. The source region is about 26 cm wide and 65 cm high and is located 19 cells (95 cm) above the bottom of the flume. The zone of flow regularisation is defined immediately leftward of the source region location, with a total width of 4 m (half a wave length).

Among the available experiments, three regular and one irregular wave tests have been simulated with the aim of testing the model's performance at large scale. The three tested water depths, and consequently three structure freeboards, have been considered for the regular wave test simulations, in order to check the model's capability under different hydraulic conditions. The characteristics of the simulated tests are summarised

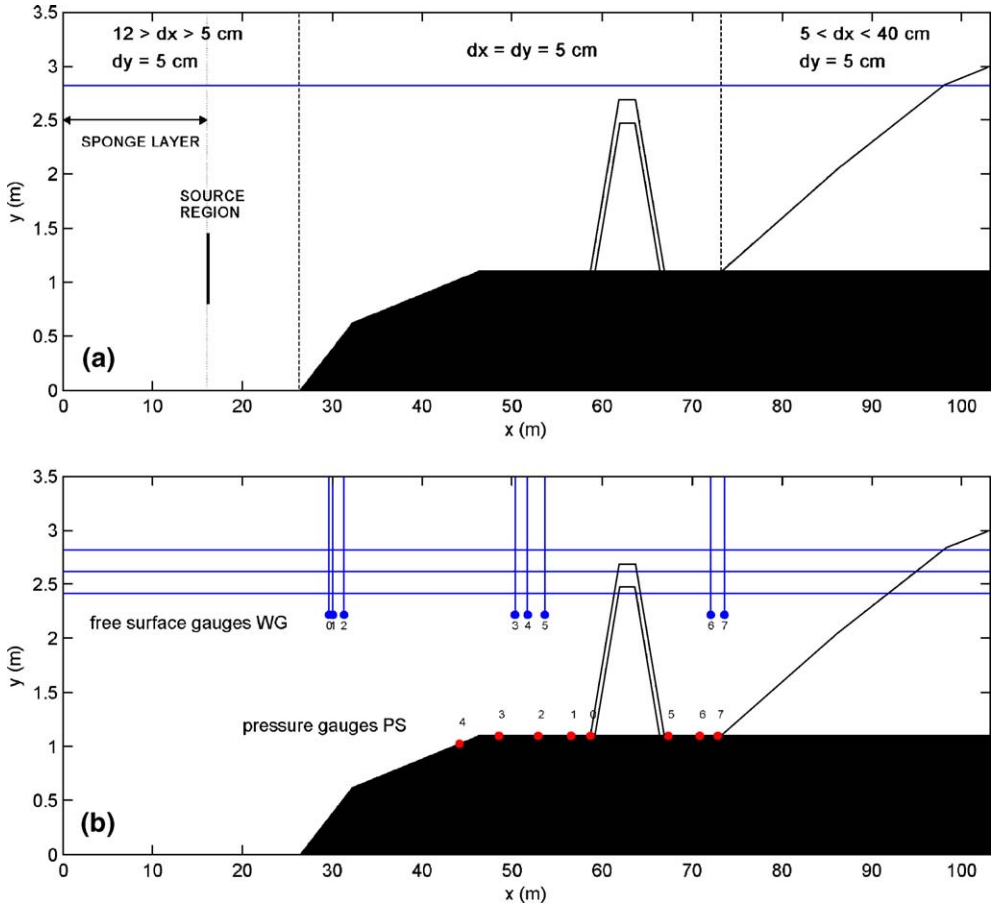

Fig. 17. Sketch of the computational mesh (axes not scaled). (a) General set-up and domain resolution, (b) tested water levels and gauges location.

in Table 2. A total of 150 s has been simulated in the case of the regular wave tests and 600 s in the case of the irregular wave simulations.

4.2. Results of regular wave simulations

Figs. 18–20 present the results of wave height envelopes and mean water level along the flume for the three regular wave tests, corresponding to $F=-13$ cm, 7 cm and 27 cm, respectively. For all the simulated tests, the pattern of wave evolution along the flume and the variations of mean water level are rather well captured by the numerical model. In the seaside zone, partial reflection at the structure induces a quasi-standing wave pattern correctly reproduced by the numerical model, with increasing wave height as the freeboard increases due to higher reflection coefficients. The root-mean-square error on the maximum wave height at the first six sections of measurement is lower than 8% for all three tests.

Table 2
Characteristics of the simulated tests

Test reference	Water depth h at paddle (m)	Freeboard F (m)	Wave height H (m)	Wave period T (s)	Crest width b (m)
R1F3C2	2.82	−0.13	0.30	2.18	1.825
R1F1C2	2.62	0.07	0.30	2.18	1.825
R1F2C2	2.42	0.27	0.30	2.18	1.825
I5F3C2	2.82	−0.13	0.40	3.58	1.825

The small perturbations of the upper envelope in the region of the crest account for wave breaking and propagation of the breaking wave until reforming in the deeper waters of the leeside zone. No data of free surface displacement are available over the breakwater crest for validation of the computed breaking pattern. Based on the numerical results and taking the maximum surface elevation as the breaking criterion, wave breaking is seen to occur, for the simulated incident wave conditions, just before the seaward edge of the structure crest (15 cm offshore of the crest edge) with a computed wave height at the breaking point of 51 cm. The large wave height in breaking and the wave envelope pattern in the crest region are consistent with the small-scale results on the no-recirculation configuration obtained by Garcia et al. (2004a). The “pumping effect” of the breaking waves induces a difference of mean water level between the protected area and the seaward zone, and thus a hydraulic gradient forcing an outflow directed seaward. In a 2DV set-up without any system of flow recirculation, the return flow forced over the structure crest affects the wave breaking conditions and induces an important steepening of the wave at breaking that can be observed in the figure. In the case of the highest value of freeboard, the breakwater is seen to be overtopped for the tested incident wave conditions

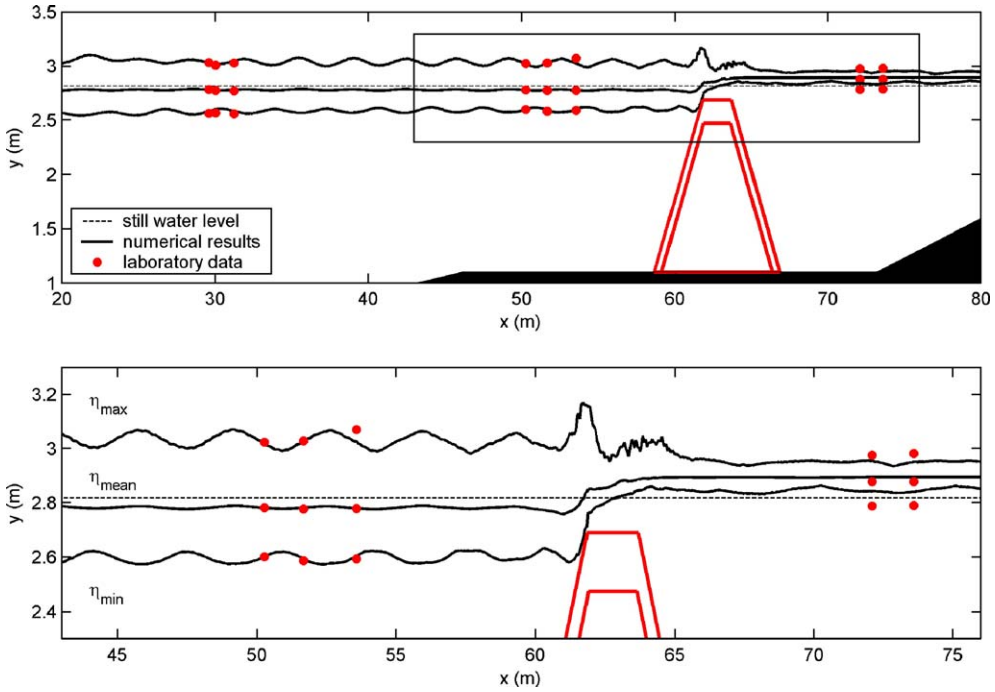

Fig. 18. Wave height envelopes and mean water level. $F=-0.13$ m, $H=0.30$ m, $T=2.18$ s, $b=1.82$ m (test R1F3C2).

but energy is not transmitted over the crest leeward side of the structure.

The degree of agreement between experimental data and numerical results is lower in the case of the leeside sections. The transmitted wave heights are underestimated. In the case of the submerged structure (Fig. 18), the numerical model predicts a reduction of maximum of wave height of about 74% while this damping rate calculated from the experimental data is no higher than 58%. The discrepancies between numerical and experimental data of wave height leeward of the breakwater may be due to disagreements in the modeling of the final permeable slope. As for all the porous media implemented in the computational domain, an accurate modeling of the final beach requires the calibration of the α and β parameters governing the porous medium internal flow. Such a calibration has not been performed as no experimental data of tests performed without breakwater to examine the behaviour of the dissipative beach in terms of reflection and dissipation are available. But the final beach is not believed to significantly influence the characteristics of the transmitted wave field, given the beach slope (parabolic profile with final slope of 3%) and its porous nature, with homogeneous natural stones of 0.5 kg. Reflection at the beach is expected to be very low (lower than 5%). Another possible explanation for the discrepancies between numerical results and experimental data in the transmission zone can be found in the parameters governing the flow inside the structure. The values considered for the present simulation result from calibration on small-scale experiments and may not be fully adequate at the larger scale. Nonetheless, the reflection performance of the breakwater, affected by the porous flow parameters, is correctly computed, as commented above. Besides, a series of numerical tests have revealed a relatively poor influence of the porous flow parameters on the obtained results of wave height envelopes.

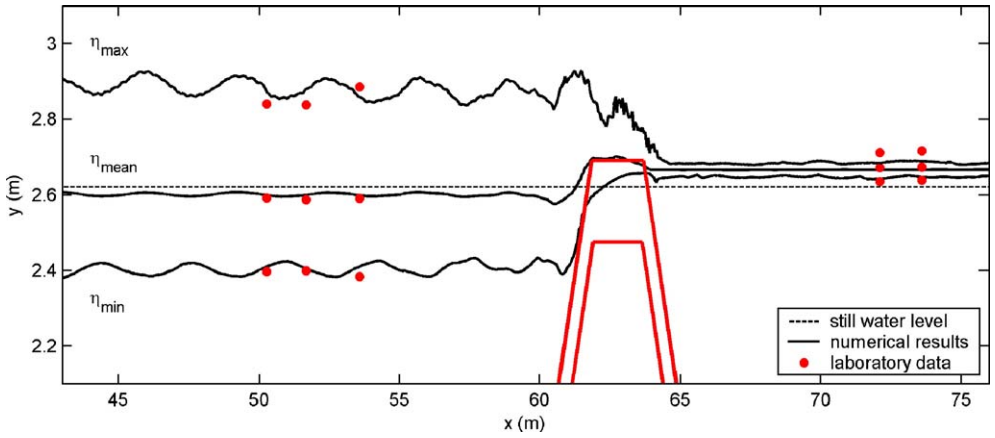

Fig. 19. Wave height envelopes and mean water level. $F=0.07$ m, $H=0.30$ m, $T=2.18$ s, $b=1.82$ m (test R1F1C2).

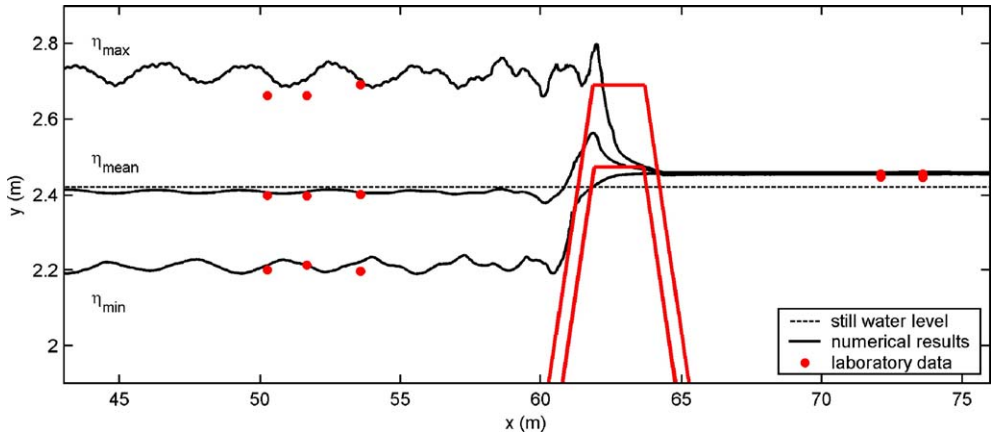

Fig. 20. Wave height envelopes and mean water level. F=0.27 m, H=0.30 m, T=2.18 s, b=1.82 m (test R1F2C2).

The tested breakwater is highly overtopped, with the contribution of the porous flow to the transmission performance being relatively low. Overtopping, controlled by the structure freeboard to incident wave height ratio, is by far the dominant transmission mechanism. The overprediction of the breakwater efficiency may finally be due to slight discrepancies between the geometric configuration of the physical model and the numerical set-up, and in particular in the definition of the structure freeboard. No measurements of the cross-section of the tested breakwater are available for comparison with the theoretical cross-section described earlier and implemented in the numerical flume. In the other two cases (Figs. 19 and 20), the maximum wave height at the leeside sections is also underestimated with respect to the experimental data. However, it is important to underline that the transmitted wave height is too small (lower than 8 cm for F=+7 cm and lower than 1 cm for F=+27 cm) for the error to be significant given the employed mesh resolution: the maximum wave height at the three leeside sections is lower than two cells for the F=+7 cm test and lower than 1 cell for the F=+27 cm test.

4.3. Preliminary results of irregular wave simulations

In this section, preliminary results of random wave simulation at large scale are presented. The considered structure is submerged, with a −13 cm freeboard. Results of free surface and pressure spectra at different locations of the wave flume are presented in Figs. 21 and 22. As can be observed, a reasonable description of the wave spectrum is achieved for both free surface and bottom pressure, in terms of general shape of the

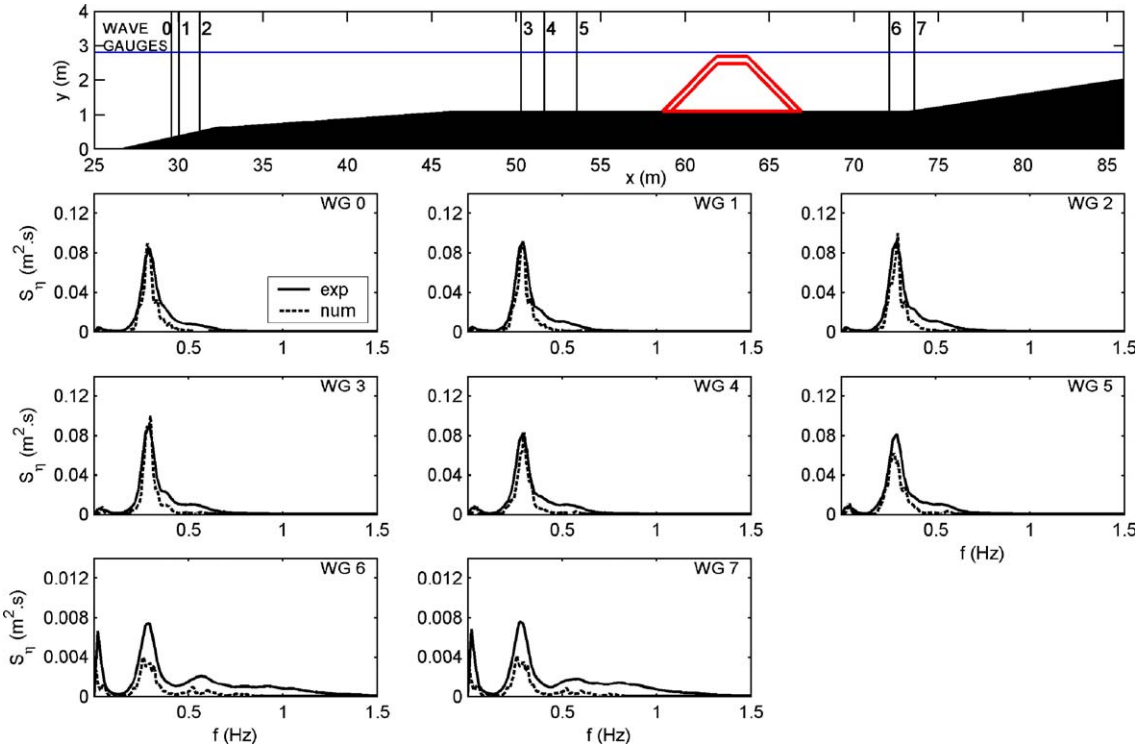

Fig. 21. Free surface spectra. F=−0.13 m, H_s=0.40 m, T_p=3.58 s, b=0.82 m, JONSWAP spectrum, γ=3.3.

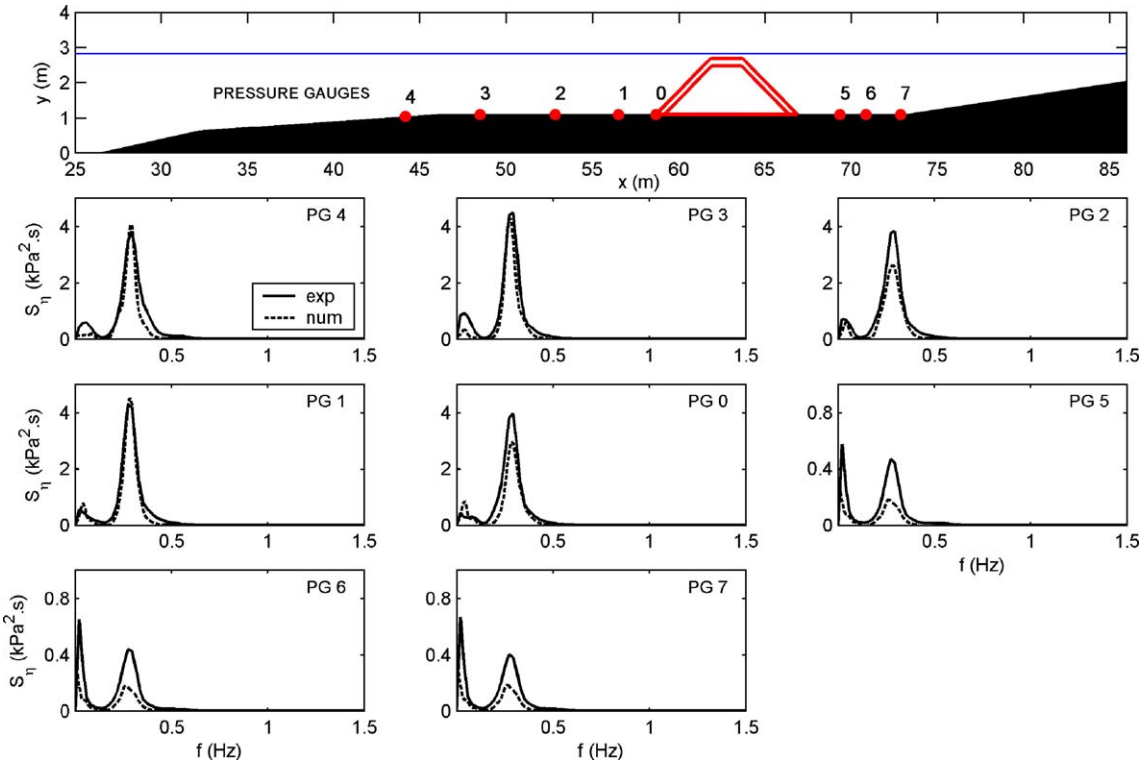

Fig. 22. Pressure spectra. $F=-0.13$ m, $H_s=0.40$ m, $T_p=3.58$ s, $b=1.82$ m, JONSWAP spectrum, $\gamma=3.3$.

spectrum and location of peak periods. In the case of the seaside sections, the energy peak and total spectral energy are rather well captured by the numerical model. In the case of the free surface displacement results, the higher frequency part of the spectrum is not accurately captured by the model, for reasons yet commented in the small-scale simulations section. The bottom pressure spectra are better reproduced by the model, as the energy carried out at the higher frequencies is very low. The transmitted wave field is not simulated by the numerical model with the same accuracy as for the seaward side. The transmitted wave energy is underestimated compared to the experimental data, as yet observed and commented in the case of the regular wave simulations. Though the shape of the wave spectra is reasonably well simulated and at all the considered sections, the frequency peak is well captured. The model is able to simulate, though rather underestimated, the low frequency energy part of the free surface and pressure spectrum, accounting for the seiche of the final part of the flume between the breakwater and the beach. As for the small-scale simulations on random waves, the model fails in accurately reproducing the high frequency part of the spectrum in the seaward region, but simulates the energy transfer to higher harmonics and the resulting broadening of the wave spectrum past the breakwater.

5. Conclusions

The simulation of irregular wave laboratory experiments with a modified version of the COBRAS model allowing the generation of wave spectra is presented. The results obtained have shown that the numerical model adequately simulates the generation and propagation of irregular wave trains over a flat bottom as well as irregular wave interaction with submerged porous breakwaters. In all the considered tests, the submerged structure is seen to induce spectral energy decay due to wave breaking over the crest and a broadening of the incident spectrum related to energy transfer to high frequencies. The results of wave spectra broadening past the structure are in agreement with previous studies by, e.g., Beji and Battjes (1993, 1994) or Losada et al. (1996a,b). The peak period of incident and transmitted wave spectra are found to be very similar.

Numerical tests were conducted on different incident wave spectra with equivalent significant wave height but different peak periods. Numerical results and experimental data are found to agree favourably in terms of wave height envelopes, mean water level, spectral shape and root-mean-square wave height. The overall trend of the spectrum transformation along the flume is well reproduced by the numerical model. The spectral width is underestimated in the seaward region: with the employed mode of wave generation, based on a source region inside the computational domain, the high frequency wave components cannot be generated together with the rest of the spectrum. The values of spectral width in the leeside region are correctly captured, confirming the model's ability to simulate the high frequency energy generation at the breakwater.

Further numerical validation has been performed considering the dynamic pressure inside the porous structure, showing for all the simulated tests a good level of agreement between the computed and measured data in terms of both pressure envelopes and pressure spectra.

Numerical results of turbulence intensity and velocity fields both around and inside the submerged structure are presented, as an example of the potentiality of the model for analysis of near-field flow characteristics that can hardly be revealed by experimental investigation. The analysis of the computed maximum velocities around the structure shows that the maximum values occur in the region of the breaking wave crest and that the velocities inside the porous media are very low for the tested structure characteristics. The largest values of turbulence intensity appear beneath the wave crest after breaking. Lower turbulence levels are observed within the structure, with values close to zero in the core. Larger values occur at the outer layer, as a result of the high vertical gradient of horizontal velocity at the structure interface. In particular, the largest values of internal turbulence are observed in the seaward vertex zone as a consequence of velocity enhancement by flow constriction. Under non-breaking waves, turbulence levels in the structure vicinity are lower and turbulence production inside the porous media is predominant. The model is found to consistently simulate the turbulence processes and flow pattern occurring in the interaction of random waves with a submerged permeable structure.

Besides, the capability of the model to reproduce large-scale laboratory experiments is investigated. Simulations of large-scale laboratory experiments have been carried out, on both regular and irregular incident wave conditions. Validation of the numerical model is performed based on measurements of free surface elevation and bottom pressure at different locations of the wave flume. The overall pattern of the wave interaction with the large-scale submerged breakwater is adequately reproduced by the numerical model. The processes of wave reflection, shoaling and breaking are correctly captured. The numerical model overestimates the breakwater performance in terms of wave damping and transmission. The underprediction of the transmitted wave height may be due to an incorrect modelling of the final permeable slope or to slight differences in the geometric uncertainties between experimental and numerical wave flumes. The predictive capabilities of the model do not seem to be significantly sensitive to a scale shift. The results achieved at a near prototype scale are promising regarding the use of the numerical model for design purposes.

Much work remains to be done, with the main objectives of future investigation being to better represent the high frequency wave components of the generated spectra, and on the other hand, to validate the model on additional laboratory tests and if possible on field measurements. But the potentialities of the employed numerical model for studies on random waves are demonstrated, which makes the model a promising tool for the analysis of the performance of low rubble-mound breakwaters in natural environments.

Acknowledgements

The authors gratefully acknowledge the funding provided by Puertos del Estado during the project “Desarrollo y explotación de un modelo numérico de interacción fluido-estructura para el estudio de funcionalidad y estabilidad de diques verticales y mixtos”.

Appendix A. Description of the irregular wave generation procedure

The definition scheme for the generation of a random wave spectrum in the modified COBRAS code consists of the following steps:

- Definition of the spectrum: JONSWAP or TMA spectra can be defined, with the input data being the significant wave height, peak period, peak enhancement factor γ and, in the case of TMA spectrum, the water depth in generation.
- Discretisation of the spectrum: the spectrum is discretised into n constant frequency bands ($n=256$ in the present work). As for the random wave spectra defined in the laboratory, cutoff frequencies are defined at 0.6 and 2.5 times the peak frequency. The energy assigned to each frequency band is corrected in order to consider the total energy of the initial full spectrum.
- Determination of wave components height and period: for each frequency band Δf_i, $i=1$ to n, the height H_i of the corresponding wave component is determined through the relation: $H_i = \sqrt{8 \cdot S_i \cdot \Delta f_i}$, with S_i the spectral density corresponding to the centre of gravity of the energy band in the frequency band (f_i, f_{i+1}). The period T_i is the inverse of the frequency value corresponding to this centre of gravity.
- Introduction of random phases: the phases p_{si} defined in Eq. (1) are determined by generating uniform, independent random numbers between $-\pi$ and π.
- Smoothing of the time series initial oscillations: in order to fulfil the zero initial condition for the mass source function: $s(t=0)=0$, a smoothing time function $f_{\text{smooth}}(t)$ and a smoothing time period T_{smooth} are introduced. The function f_{smooth} is 0 at $t=0$, linearly increases up to 1 for $0<t\le T_{\text{smooth}}$, and is constant and equal to 1 for $t>T_{\text{smooth}}$.
- Introduction of input data for simulation: the triplet ($H_{i=1}=0$, $T_{i=1}=T_{\text{smooth}}$, $p_{si}=0$) is the first input data. The following data are the above defined triplets (H_i, T_i, p_{si}), $i=2$ to $n+1$.

References

Avgeris, I., Karambas, T.V, Prinos, P., 2004. Boussinesq modeling of wave interaction with porous submerged breakwaters. Proceedings of the 29th International Conference in Coastal Engineering. World Scientific, pp. 604–616.

Beji, S., Battjes, J.A., 1993. Experimental investigation of nonlinear wave propagation over a bar. Coastal Engineering 19, 151–162.

Beji, S., Battjes, J.A., 1994. Numerical simulation of nonlinear wave propagation over a bar. Coastal Engineering 23, 1–16.

Cox, D.T., Kobayashi, N., Kriebel, D.L., 1994. Numerical model verification using SUPERTANK data in surf and swash zones. Proceedings of Coastal Dynamics’94. ASCE, pp. 248–262.

Denny, M.W., 1988. Biology and the Mechanics of the Wave-Swept Environment. Princeton University Press, Princeton, NJ, USA.

Garcia, N., Lara, J.L., Losada, I.J., 2004a. 2-D numerical analysis of near-field flow at low-crested breakwaters. Coastal Engineering 51 (10), 991–1020.

Garcia, N., Lara, J.L., Lomonaco, P., Losada, I.J., 2004b. Flow at low-crested breakwaters under breaking conditions. Proceedings of the 29th International Conference on Coastal Engineering. World Scientific, pp. 4240–4252.

Hsu, T.-J., Sakakiyama, T., Liu, P.L.-F., 2002. A numerical model for wave motions and turbulence flows in front of a composite breakwater. Coastal Engineering 46, 25–50.

Iwata, K., Kawasaki, K., Kim, D.S., 1996. Breaking limit, breaking and post-breaking wave deformation due to submerged structures. Journal of Geophysical Research 88 (C10), 5925–5938.

Karambas, T.V., Prinos, P., Kriezi, E.E., 1997. Modeling of hydrodynamic and morphological effects of submerged breakwaters on the nearshore region. Proceedings of Coastal Dynamics '97. ASCE, pp. 764–773.

Kawasaki, K., 1999. Numerical simulation of breaking and post-breaking wave deformation process around a submerged breakwater. Coastal Engineering Journal 41, 201–223.

Kobayashi, N., Wurjanto, A., 1989. Wave transmission over submerged breakwaters. Journal of Waterway, Port, Coastal, and Ocean Engineering, ASCE 115 (5), 662–680.

Kobayashi, N., Wurjanto, A., 1990. Numerical model for waves on rough permeable slopes. Special Issue No. 7 on Rational Design of Mound Structures. Journal of Coastal Research 149–166.

Kobayashi, N., Cox, D.T., Wurjanto, A., 1992. Irregular wave reflection and runup on rough impermeable slopes. Journal of Waterway, Port, Coastal, and Ocean Engineering, ASCE 116 (6), 708–726.

Li, Tingqiu, Troch, P., De Rouck, J., 2004. Wave overtopping over a dike. Journal of Computational Physics 198, 686–726.

Lin, P., Liu, P.L.-F., 1998. A numerical study of breaking waves in the surf zone. Journal of Fluid Mechanics 359, 239–264.

Lin, P., Liu, P.L.-F., 1999. Internal wave-maker for Navier–Stokes equations models. Journal of Waterway, Port, Coastal, and Ocean Engineering 125 (4), 207–217.

Longuet-Higgins, M.S., 1975. On the distribution of the periods and the amplitudes of sea waves. Journal of Geophysical Research 86 (C5), 4299–4301.

Losada, I.J., Silva, R., Losada, M.A., 1996a. Interaction of non-breaking directional random waves with submerged breakwaters. Coastal Engineering 28, 249–266.

Losada, I.J., Silva, R., Losada, M.A., 1996b. 3-D non-breaking regular wave interaction with submerged breakwaters. Coastal Engineering 28, 229–248.

Losada, I.J., Lara, J.L., Garcia, N., 2003. 2-D experimental and numerical analysis of wave interaction with low-crested breakwaters including breaking and flow recirculation. Proceedings of Coastal Structures'03. ASCE, pp. 863–875.

Massel, S.R., Butowski, P., 1980. Wind waves transmission through porous breakwater. Proceedings of the 17th International Conference on Coastal Engineering. ASCE, pp. 333–346.

Massel, S.R., Mei, C.C., 1977. Transmission of random wind waves through perforated or porous breakwaters. Coastal Engineering 1 (1), 63–78.

Rojanakamthorn, S., Isobe, M., Watanabe, A., 1989. A mathematical model of wave transformation over a submerged breakwater. Coastal Engineering in Japan 32 (2), 209–234.

Rojanakamthorn, S., Isobe, M., Watanabe, A., 1990. Modeling of wave transformation on submerged breakwater. Proceedings of the 22nd International Conference in Coastal Engineering. ASCE, pp. 1060–1073.

Schaffer, H.A., Madsen, P.A., 1995. Further enhancements of Boussinesq-type equations. Coastal Engineering 26 (1), 1–14.

Troch, P., de Rouck, J., 1998. Development of two-dimensional numerical wave flume for wave interaction with rubble mound breakwaters. Proceedings of the 26th International Conference of Coastal Engineering. ASCE, pp. 1638–1649.

Van Gent, M.R.A., 1994. The modelling of wave action on and in coastal structures. Coastal Engineering 22, 311–339.

Van Vledder, G.P., 1992. Statistics of wave group parameters. Proceedings of the 23rd International Conference of Coastal Engineering. ASCE, pp. 946–959.

Vidal, C., Losada, I.J., Martín, F.L., 1998. Stability of near-bed rubble-mound structures. Proceedings of the 26th International Conference of Coastal Engineering. ASCE, pp. 1730–1743.

Wei, G., Kirby, J.T., Sinha, A., 1999. Generation of waves in Boussinesq models using a source function method. Coastal Engineering 36 (4), 271–299.

Yoshida, A., Murakami, K., Yamashiro, M., Kojima, H., 1996. Second-order interaction between random wave and submerged obstacle. Proceedings of the 25th International Conference of Coastal Engineering. ASCE, pp. 927–940.